antibody (HPA038016) and mouse anti-β-actin (A5441) were from Sigma (St Louis, MO, USA).

Transfection of siRNA

AJUBA, LIMD1, WTIP, LATS1, LATS2 and control small interfering RNAs (ON-TARGETplus SMARTpool siRNA reagent, Thermo Fisher Scientific, Lafayette, CO, USA) were introduced into cells by transient transfection with RNAi MAX (Invitrogen) in accordance with the manufacturer's instructions.

Cell proliferation assay

MM cells (1×10^4) were seeded on flat-bottomed 24-well plates. After 24 h, cells were transduced with lentiviral vectors, and then incubated for an additional 48 h. Cells were incubated to grow for an additional 5 days under Blasticidin (InvivoGen, San Diego, CA, USA) selection. The medium was then changed with fresh RPMI-1640 medium with 1% FCS as described previously.[19] As an exceptional case, Y-MESO-8D cells were cultured in fresh RPMI-1640 medium with 5% FCS because this cell line hardly grew in the 1% FCS medium. After an additional 24 h incubation, calorimetric assays were performed by adding 30 μl of Tetra Color One (Seikagaku, Tokyo, Japan) containing 2-(2-methoxy-4-nitrophenyl)-3-(4-nitrophenyl)-5-(2,4-disulfo
phenyl)-2H-tetrazolium, monosodium salt and 1-methoxy-5-methylphena
zinium methylsulfate as electron carrier in each well and incubated at 37 °C for 1 h. Absorbance was measured at 450 nm using a multiplate reader. Cell proliferation was shown as a relative ratio to control cells.

Anchorage-independent growth in soft agar

Bottom agar was made of 1.5 ml of 0.5% agar supplemented with 10% FCS and RPMI-1640 medium, plated in 35 mm plates. Cells (3.0×10^4) were mixed with 1.0 ml of 0.35% agar supplemented with 10% FCS and RPMI-1640 medium, and then added onto the bottom agar. Cells were incubated to grow and form colonies for 12 days. Colonies were stained with 0.03% crystal violet, and the numbers of colonies were counted.

CONFLICT OF INTEREST

The authors declare no conflict of interest.

ACKNOWLEDGEMENTS

This work was supported in part by KAKENHI (24650650, 25290053), Grants-in-Aid for Third-Term Comprehensive Control Research for Cancer from the Ministry of Health, Labor and Welfare of Japan, P-DIRECT and the Takeda Science Foundation (YS). We thank Dr Adi F Gazdar for the cell lines and Mari Kizuki and Miwako Nishizawa for their excellent technical assistance. IT was supported by the Foundation for Promotion of Cancer Research.

REFERENCES

1 Pass HI, Vogelzang N, Hahn S, Carbone M. Malignant pleural mesothelioma. *Curr Probl Cancer* 2004; **28**: 93–174.
2 Yang H, Testa JR, Carbone M. Mesothelioma epidemiology, carcinogenesis, and pathogenesis. *Curr Treat Options Oncol* 2008; **9**: 147–157.
3 Delgermaa V, Takahashi K, Park EK, Le GV, Hara T, Sorahan T *et al.* Global mesothelioma deaths reported to the World Health Organization between 1994 and 2008. *Bull World Health Organ* 2011; **89**: 716–724.
4 Carbone M, Ly BH, Dodson RF, Pagano I, Morris PT, Dogan UA *et al.* Malignant mesothelioma: facts, myths, and hypotheses. *J Cell Physiol* 2012; **227**: 44–58.
5 Robinson BW, Lake RA. Advances in malignant mesothelioma. *N Engl J Med* 2005; **353**: 1591–1603.
6 Robinson BW, Musk AW, Lake RA. Malignant mesothelioma. *Lancet* 2005; **366**: 397–408.
7 Vogelzang NJ, Rusthoven JJ, Symanowski J, Denham C, Kaukel E, Ruffie P *et al.* Phase III study of pemetrexed in combination with cisplatin versus cisplatin alone in patients with malignant pleural mesothelioma. *J Clin Oncol* 2003; **21**: 2636–2644.
8 Carbone M, Kratzke RA, Testa JR. The pathogenesis of mesothelioma. *Semin Oncol* 2002; **29**: 2–17.
9 Sekido Y. Genomic abnormalities and signal transduction dysregulation in malignant mesothelioma cells. *Cancer Sci* 2010; **101**: 1–6.
10 Bianchi AB, Mitsunaga SI, Cheng JQ, Klein WM, Jhanwar SC, Seizinger B *et al.* High frequency of inactivating mutations in the neurofibromatosis type 2 gene (NF2) in primary malignant mesotheliomas. *Proc Natl Acad Sci USA* 1995; **92**: 10854–10858.
11 Sekido Y, Pass HI, Bader S, Mew DJ, Christman MF, Gazdar AF *et al.* Neurofibromatosis type 2 (NF2) gene is somatically mutated in mesothelioma but not in lung cancer. *Cancer Res* 1995; **55**: 1227–1231.
12 Dong J, Feldmann G, Huang J, Wu S, Zhang N, Comerford SA *et al.* Elucidation of a universal size-control mechanism in *Drosophila* and mammals. *Cell* 2007; **130**: 1120–1133.
13 Saucedo LJ, Edgar BA. Filling out the Hippo pathway. *Nat Rev Mol Cell Biol* 2007; **8**: 613–621.
14 Huang J, Wu S, Barrera J, Matthews K, Pan D. The Hippo signaling pathway coordinately regulates cell proliferation and apoptosis by inactivating Yorkie, the *Drosophila* Homolog of YAP. *Cell* 2005; **122**: 421–434.
15 Tapon N, Harvey KF, Bell DW, Wahrer DC, Schiripo TA, Haber D *et al.* Salvador promotes both cell cycle exit and apoptosis in *Drosophila* and is mutated in human cancer cell lines. *Cell* 2002; **110**: 467–478.
16 Badouel C, Garg A, McNeill H. Herding Hippos: regulating growth in flies and man. *Curr Opin Cell Biol* 2009; **21**: 837–843.
17 Zhao B, Ye X, Yu J, Li L, Li W, Li S *et al.* TEAD mediates YAP-dependent gene induction and growth control. *Genes Dev* 2008; **22**: 1962–1971.
18 Mizuno T, Murakami H, Fujii M, Ishiguro F, Tanaka I, Kondo Y *et al.* YAP induces malignant mesothelioma cell proliferation by upregulating transcription of cell cycle-promoting genes. *Oncogene* 2012; **31**: 5117–5122.
19 Yokoyama T, Osada H, Murakami H, Tatematsu Y, Taniguchi T, Kondo Y *et al.* YAP1 is involved in mesothelioma development and negatively regulated by Merlin through phosphorylation. *Carcinogenesis* 2008; **29**: 2139–2146.
20 Murakami H, Mizuno T, Taniguchi T, Fujii M, Ishiguro F, Fukui T *et al.* LATS2 is a tumor suppressor gene of malignant mesothelioma. *Cancer Res* 2011; **71**: 873–883.
21 Feng Y, Longmore GD. The LIM protein Ajuba influences interleukin-1-induced NF-kappaB activation by affecting the assembly and activity of the protein kinase Czeta/p62/TRAF6 signaling complex. *Mol Cell Biol* 2005; **25**: 4010–4022.
22 Locasale JW, Shaw AS, Chakraborty AK. Scaffold proteins confer diverse regulatory properties to protein kinase cascades. *Proc Natl Acad Sci USA* 2007; **104**: 13307–13312.
23 Shaw AS, Filbert EL. Scaffold proteins and immune-cell signalling. *Nat Rev Immunol* 2009; **9**: 47–56.
24 Levchenko A, Bruck J, Sternberg PW. Scaffold proteins may biphasically affect the levels of mitogen-activated protein kinase signaling and reduce its threshold properties. *Proc Natl Acad Sci USA* 2000; **97**: 5818–5823.
25 Burack WR, Shaw AS. Signal transduction: hanging on a scaffold. *Curr Opin Cell Biol* 2000; **12**: 211–216.
26 Abe Y, Ohsugi M, Haraguchi K, Fujimoto J, Yamamoto T. LATS2-Ajuba complex regulates gamma-tubulin recruitment to centrosomes and spindle organization during mitosis. *FEBS Lett* 2006; **580**: 782–788.
27 Das Thakur M, Feng Y, Jagannathan R, Seppa MJ, Skeath JB, Longmore GD *et al.* Ajuba LIM proteins are negative regulators of the Hippo signaling pathway. *Curr Biol* 2010; **20**: 657–662.
28 Zhao B, Wei X, Li W, Udan RS, Yang Q, Kim J *et al.* Inactivation of YAP oncoprotein by the Hippo pathway is involved in cell contact inhibition and tissue growth control. *Genes Dev* 2007; **21**: 2747–2761.
29 Oh HJ, Lee KK, Song SJ, Jin MS, Song MS, Lee JH *et al.* Role of the tumor suppressor RASSF1A in Mst1-mediated apoptosis. *Cancer Res* 2006; **66**: 2562–2569.
30 Polesello C, Huelsmann S, Brown NH, Tapon N. The *Drosophila* RASSF homolog antagonizes the hippo pathway. *Curr Biol* 2006; **16**: 2459–2465.
31 Sasaki H. Mechanisms of trophectoderm fate specification in preimplantation mouse development. *Dev Growth Differ* 2010; **52**: 263–273.
32 Alvarez-Fernandez M, Halim VA, Krenning L, Aprelia M, Mohammed S, Heck AJ *et al.* Recovery from a DNA-damage-induced G2 arrest requires Cdk-dependent activation of FoxM1. *EMBO Rep* 2010; **11**: 452–458.
33 Laoukili J, Stahl M, Medema RH. FoxM1: at the crossroads of ageing and cancer. *Biochim Biophys Acta* 2007; **1775**: 92–102.
34 Wang IC, Chen YJ, Hughes D, Petrovic V, Major ML, Park HJ *et al.* Forkhead box M1 regulates the transcriptional network of genes essential for mitotic progression and genes encoding the SCF (Skp2-Cks1) ubiquitin ligase. *Mol Cell Biol* 2005; **25**: 10875–10894.
35 Fu Z, Malureanu L, Huang J, Wang W, Li H, van Deursen JM *et al.* Plk1-dependent phosphorylation of FoxM1 regulates a transcriptional programme required for mitotic progression. *Nat Cell Biol* 2008; **10**: 1076–1082.

36 Wang IC, Chen YJ, Hughes DE, Ackerson T, Major ML, Kalinichenko VV *et al.* FoxM1 regulates transcription of JNK1 to promote the G1/S transition and tumor cell invasiveness. *J Biol Chem* 2008; **283**: 20770–20778.
37 Wang Z, Banerjee S, Kong D, Li Y, Sarkar FH. Down-regulation of Forkhead Box M1 transcription factor leads to the inhibition of invasion and angiogenesis of pancreatic cancer cells. *Cancer Res* 2007; **67**: 8293–8300.
38 Hirota T, Kunitoku N, Sasayama T, Marumoto T, Zhang D, Nitta M *et al.* Aurora-A and an interacting activator, the LIM protein Ajuba, are required for mitotic commitment in human cells. *Cell* 2003; **114**: 585–598.
39 Ferrand A, Chevrier V, Chauvin JP, Birnbaum D. Ajuba: a new microtubule-associated protein that interacts with BUBR1 and Aurora B at kinetochores in metaphase. *Biol Cell* 2009; **101**: 221–235.
40 Benzinger A, Muster N, Koch HB, Yates 3rd JR, Hermeking H. Targeted proteomic analysis of 14-3-3 sigma, a p53 effector commonly silenced in cancer. *Mol Cell Proteomics* 2005; **4**: 785–795.
41 Mo JS, Yu FX, Gong R, Brown JH, Guan KL. Regulation of the Hippo-YAP pathway by protease-activated receptors (PARs). *Genes Dev* 2012; **26**: 2138–2143.
42 Yu FX, Zhao B, Panupinthu N, Jewell JL, Lian I, Wang LH *et al.* Regulation of the Hippo-YAP pathway by G-protein-coupled receptor signaling. *Cell* 2012; **150**: 780–791.
43 Zhao B, Li L, Wang L, Wang CY, Yu J, Guan KL *et al.* Cell detachment activates the Hippo pathway via cytoskeleton reorganization to induce anoikis. *Genes Dev* 2012; **26**: 54–68.
44 Boggiano JC, Fehon RG. Growth control by committee: intercellular junctions, cell polarity, and the cytoskeleton regulate Hippo signaling. *Dev Cell* 2012; **22**: 695–702.
45 Wada K, Itoga K, Okano T, Yonemura S, Sasaki H. Hippo pathway regulation by cell morphology and stress fibers. *Development* 2011; **138**: 3907–3914.
46 Sansores-Garcia L, Bossuyt W, Wada K, Yonemura S, Tao C, Sasaki H *et al.* Modulating F-actin organization induces organ growth by affecting the Hippo pathway. *EMBO J* 2011; **30**: 2325–2335.
47 Marie H, Pratt SJ, Betson M, Epple H, Kittler JT, Meek L *et al.* The LIM protein Ajuba is recruited to cadherin-dependent cell junctions through an association with alpha-catenin. *J Biol Chem* 2003; **278**: 1220–1228.
48 Fujii M, Toyoda T, Nakanishi H, Yatabe Y, Sato A, Matsudaira Y *et al.* TGF-beta synergizes with defects in the Hippo pathway to stimulate human malignant mesothelioma growth. *J Exp Med* 2012; **209**: 479–494.

Supplementary Information accompanies this paper on the Oncogene website (http://www.nature.com/onc)

IJC
International Journal of Cancer

Expression of chromobox homolog 7 (CBX7) is associated with poor prognosis in ovarian clear cell adenocarcinoma *via* TRAIL-induced apoptotic pathway regulation

Kanako Shinjo[1,2], Yoriko Yamashita[1,3], Eiko Yamamoto[2], Shinya Akatsuka[1], Nozomi Uno[1], Akihiro Kamiya[3], Kaoru Niimi[2], Yuka Sakaguchi[2], Tetsuro Nagasaka[4], Takashi Takahashi[5], Kiyosumi Shibata[2], Hiroaki Kajiyama[2], Fumitaka Kikkawa[2] and Shinya Toyokuni[1]

[1] Department of Pathology and Biological Responses, Nagoya University Graduate School of Medicine, Showa-ku, Nagoya, Japan
[2] Department of Obstetrics and Gynecology, Nagoya University Graduate School of Medicine, Showa-ku, Nagoya, Japan
[3] Department of Experimental Pathology and Tumor Biology, Nagoya City University Graduate School of Medical Sciences, Mizuho-ku, Nagoya, Japan
[4] Department of Pathophysiological Laboratory Sciences, Nagoya University Graduate School of Medicine, Higashi-ku, Nagoya, Japan
[5] Division of Molecular Carcinogenesis, Center for Neurological Diseases and Cancer, Nagoya University Graduate School of Medicine, Showa-ku, Nagoya, Japan

Cancer Cell Biology

Ovarian cancer is the most lethal gynecologic malignancy, and clear cell adenocarcinoma of the ovary (OCCA), in particular, has a relatively poor prognosis among the ovarian cancer subtypes because of its high chemoresistance. Chromobox (CBX) 7 is a polycomb repressive complex 1 component that prolongs the lifespan of normal human cells by downregulating the INK4a/ARF expression which promotes cell-cycle progression. However, recent reports studying the relationship between CBX7 expression and patient survival have differed regarding the tumor cell origins, and the precise role of CBX7 in human carcinomas remains obscure. In this study, we analyzed CBX7 expression by immunohistochemistry in 81 OCCA patients and evaluated its association with their clinical outcomes. Both the overall and progression-free survival rates of the CBX7-positive patients were significantly shorter than those of the CBX7-negative patients ($p < 0.05$). CBX7 knockdown experiments using two OCCA cell lines, TOV21G and KOC-7C, revealed that cell viability was significantly reduced compared to the control cells ($p < 0.001$). Expression microarray analysis revealed that apoptosis-related genes, particularly tumor necrosis factor-related apoptosis-inducing ligand (TRAIL), were significantly upregulated in CBX7 knockdown cells ($p < 0.01$). We further confirmed that CBX7 knockdown resulted in TRAIL-induced apoptosis in the OCCA cells. Thus, in this study, we showed for the first time that CBX7 was associated with a decreased OCCA prognosis. We also successfully demonstrated that the TRAIL pathway is a novel target for CBX7 expression modulation in these cells, and therapeutic agents utilizing the TRAIL pathway may be particularly effective for targeted OCCA therapy.

Ovarian cancer is the most lethal gynecologic malignancy. There is no effective screening method, and most women are diagnosed with advanced-stage disease. In Japan, ovarian clear cell adenocarcinoma (OCCA) accounts for ~25% of all epithelial ovarian cancer (EOC) cases,[1] whereas in North America and Europe, OCCA accounts for only 1–12% of cases.[2] OCCA has been considered to be distinct from high-grade serous adenocarcinoma because of its clinical and biological characteristics. OCCA has been known to be associated with endometriosis,[3,4] and recent studies have suggested that oxidative stress caused by excess iron leads to carcinogenesis in the ovary.[5,6] Advanced stage is associated with poor prognosis in OCCA,[2] and the survival rates in the stages are poorer than those for patients with serous adenocarcinoma,[7] most likely because of OCCA resistance to standard platinum-based chemotherapy.[8] Therefore, it is important to find new therapeutic targets for OCCA.

Chromobox 7 (CBX7) is a member of the polycomb group (PcG) of proteins and is a component of polycomb repressive complex 1 (PRC1). PRC1 can silence the genes that are related to stem cell renewal, differentiation and cancer in conjunction with PRC2.[9] PcG proteins have been reported to be overexpressed and associated with tumorigenesis in a variety of human cancers, mostly by downregulating

Key words: ovarian clear cell adenocarcinoma, chromobox homolog 7 (CBX7), immunohistochemistry, siRNA, expression microarray, TNFSF10 (TRAIL)
Additional Supporting Information may be found in the online version of this article
Grant sponsor: Scientific Research from the Japan Society for the Promotion of Science; **Grant number:** 23590394 (to Y.Y.)
DOI: 10.1002/ijc.28692
History: Received 23 May 2013; Accepted 11 Dec 2013; Online 22 Dec 2013
Correspondence to: Yoriko Yamashita, Department of Experimental Pathology and Tumor Biology, Nagoya City University Graduate School of Medical Sciences, 1 Kawasumi, Mizuho-cho, Mizuho-ku, Nagoya, 467-8601, Japan, Tel.:+81-52-853-8146, Fax: +81-52-842-0817, E-mail: k46581a@nucc.cc.nagoya-u.ac.jp

What's new?

Ovarian cancer is the most lethal gynecologic malignancy, with clear celladenocarcinoma of the ovary (OCCA) having a particularly poor prognosis due to high chemoresistance. Chromobox homolog 7 (CBX7) is a polycomb group transcriptional repressor whose role in human cancer remains controversial. Here, the authors showed for the first time that CBX7 expression is related to worse prognosis in OCCA. Furthermore, knockdown of CBX7 *in vitro* induced apoptosis in OCCA cell lines, possibly via regulation of the TRAIL-pathway. The findings thus indicate CBX7 as a good prognostic marker, andthe TRAIL-pathway as a potential target for OCCA diagnosis and therapy.

the tumor suppressor genes.[10] CBX7 has been reported to extend the cellular life span by directly repressing the INK4a/ARF locus.[11] Additionally, CBX7 is an oncogene in several human tumors, including follicular lymphoma, prostate and gastric cancers.[12–14] In follicular lymphoma, CBX7 also cooperates with MYC to produce highly aggressive B-cell lymphoma and can initiate T-cell lymphomagenesis by repressing the INK4a/ARF locus.[13] Recently, it has been reported that CDKN2B-AS (ANRIL), a long noncoding RNA also encoded in the INK4a/ARF locus, acts together with CBX7 to repress INK4a/ARF locus genes, such as CDKN2A (p16; p16INK4a) and ARF (p14 ARF) in prostate cancer cells.[15] Furthermore, a genome-wide association study comparing Japanese women with endometriosis to healthy controls revealed that a single nucleotide polymorphism that showed the strongest association with endometriosis was located in the intron of the ANRIL gene.[16] As OCCA is known to have strong association with endometriosis,[4–6] we speculated that CBX7 and ANRIL may play some important roles in the OCCA tumorigenesis. However, in clear contrast, the loss of CBX7 expression has been reported in association with poorer prognoses and more aggressive behaviors of pancreatic, colorectal, and lung cancers.[17–19] It has been shown that CBX7 represses CDH1 (E-cadherin) expression and CCNE1 (cyclin E1) expression in pancreatic and lung cancers, respectively.[20,21] Therefore, the role of CBX7 in cancer still remains controversial. In this study, we attempted to clarify the role of CBX7 in ovarian cancer, specifically OCCA.

Material and Methods

Patients and tissue samples

The ethics committee (Internal Review Board) of the Nagoya University Graduate School of Medicine approved the experiments. The human samples were obtained after each patient provided written informed consent. Formalin-fixed, paraffin-embedded tumor samples from 81 primary OCCA were obtained from the patients who underwent surgical treatment at Nagoya University Hospital from 1986 to 2009 and had clinical follow-up information available. Tumor staging was based on the International Federation of Gynecology and Obstetrics (FIGO) classifications, and reviewed by two expert gynecologists (H.K. and F.K.) for this study. All patients were primarily treated with optimally debulking surgery by skilled surgeons in gynecologic oncology. Thereafter, 75 (93%) of the 81 patients received adjuvant chemotherapy. Beginning in 1997, most of the patients received platinum- and taxane-based agents or CPT-11 chemotherapy. Before 1997, various cisplatin-based chemotherapies were administered. The following chemotherapy regimens were followed: 7% cyclophosphamide 500 mg/m^2, adriamycin 50 mg/m^2, and cisplatin 50 mg/m^2 (CAP), 8% cisplatin and carboplatin (PP), 5% cisplatin, vinblastine, and bleomycin (PVB), 62% paclitaxel 175 mg/m^2, carboplatin AUC5 (TC), 3% docetaxel 70 mg/m^2, carboplatin AUC5 (DC), 4% CPT-11 180 mg/m^2, cisplatin 60 mg/m^2 (CPT-P), 2% other, and 9% unknown. Tumor recurrence or progression was determined by clinical, radiologic, or histologic diagnosis. All histologic diagnoses were specifically reviewed by experts in gynecological pathology (Y.Y. and T.N.) for this study. Endometriosis was defined histologically as the presence of endometrial glands and stromal tissues other than the endometrium or within onethird depth of the uterine myometrium. We also excluded ovarian endometrial cysts lacking epithelium without any atypia for the diagnosis of endometriosis.

Cell culture and cell lines

The human OCCA cell line TOV-21G and a prostate cancer PC3 line were obtained from the American Type Culture Collection (ATCC, Manassas, VA), and the KOC7C line was a generous gift from Dr. Junzo Kigawa (Tottori University, Tottori, Japan). These cells were cultured in an RPMI-1640 medium (Sigma-Aldrich, St Louis, MO) containing 10% fetal bovine serum at 37°C under a 5% CO_2 atmosphere and were tested and authenticated using the short tandem repeat (STR) method.[22] Human OCCA cell lines JHOC-5, 7, 8, 9 were recently (2009-) obtained from Riken BRC (Tsukuba, Japan) and cultured using Dulbecco's Modified Eagle's Medium/Nutrient F-12 Ham (DMEM:F12) medium (Sigma-Aldrich) with similar conditions. Human endometrial epithelial cells were obtained from normal endometrium of a patient undergoing hysterectomy, and after collagenase treatment, cells were cultured using DMEM:F12 and then infected first with a lentivirus encoding HPV16 E6 and E7 followed by a retrovirus encoding human telomerase similar to previous studies.[23,24] Establishment procedure for the cells (hEEC-N1) was done with written permission, and established cells were confirmed as endometrial epithelial origin by immunohistochemical

analyses for detection of both keratin and vimentin using similar methods as a previous study.[23]

Immunohistochemistry and RNA fluorescence *in situ* hybridization (RNA-FISH)

For immunohistochemistry (IHC), we used anti-CBX7 (ab21873, Abcam, Cambridge, MA) as the primary antibody. DNA probes for RNA-FISH were prepared by PCR amplifying cDNA templates to obtain ~500 bp sized-PCR products using primers 5′-GAATTTGGGAATGAGGAGCA-3′ and 5′-AAGCTGCAAAGGCCTCAATA-3′ for ANRIL and 5′-TCAG AAGGATTCCTATGTGG-3′ and 5′-TCTCCTTAATGTCAC GCACG-3′ for human β-actin, and then labeled with SpectrumOrange using Vysis Nick Translation Kit (Abbott, Abbott Park, IL). For fluorescence IHC and RNA fluorescence *in situ* hybridization (RNA-FISH), cells were grown on a chamber slide, and fixed with 4% paraformaldehyde. For RNA-FISH, after permeabilization using cytoskeletal buffer, slides were hybridized with the labeled probes. For fluorescence IHC, cells were visualized with Alexa Fluor labeled secondary antibody (Life Technologies, Carlsbad, CA). Finally, cells were counterstained with DAPI and then visualized with a fluorescence microscope.

For formalin-fixed, paraffin-embedded ovarian tumor sections, we used polymer-based methods with the EnVision System (DAKO, Glostrup, Denmark). CBX7 staining was interpreted by three independent pathologists (Y.Y., T.N., and S.T.) blinded to clinical data. Because interobserver variability was rather large in samples with 10–50% nuclear staining, we defined the samples that contained nuclear staining >10% of cancer cells as positive, and the others negative.

Small interference RNA (siRNA) transfection

To knockdown CBX7, we used two individual siRNAs: One was an endoribonuclease-prepared siRNA (esiRNA) against CBX7 (EHU035461, Sigma-Aldrich), and the other was designed using the sense sequence 5′-GCATTTGCCCATC TGCCTT-3′; we named these siRNAs siCBX7-1 and siCBX7-2, respectively. We used MISSION siRNA Universal Negative Control (SIC-001, Sigma-Aldrich) as the negative control. KOC7C and TOV21G were transfected with the siRNAs using the Lipofectamine RNAiMAX reagent (Invitrogen, Carlsbad, CA) at a final concentration of 10 nM, according to the manufacturer's instructions. Analyses were performed 48 hr after transfection.

Quantitative reverse transcriptase-PCR

Total RNA was extracted from the cell lines using the RNeasy Plus Mini Kit (QIAGEN, Hilden, Germany) according to the manufacturer's instructions. Then, cDNA was synthesized from 500 ng total RNA using the Superscript III First-Strand Synthesis System for RT-PCR (Life Technologies), and quantitative PCR was performed as previously described.[25] The sequences of primers were as follows: CBX7, forward 5′-GGATGGCCCCCAAAGTACAG-3′ and reverse 5′-TATACCCCGATGCTCGGTCTC-3′; ANRIL, forward 5′-CAACATCCACCACTGGATCTTAACA-3′ and reverse 5′-AG CTTCGTATCCCCAATGAGATACA-3′; CDKN2A, forward 5′-CATAGATGCCGCGGAAGGT-3′ and reverse 5′-CCCGA GGTTTCTCAGAGCCT-3′; TNFSF10A, forward 5′-C CTCA GAGAGTAGCAGCTCACA-3′ and reverse 5′-GCCCA GAG CCTTTTCATTC-3′; for β-actin, forward 5′-CGGGAC CT GACTGACTA-3′ and reverse 5′-GAAGGAAGGCTGGA AG AGT-3′; and TNFSF10, forward 5′-CCTCAGAGAGTAG CA GCTCACA-3′ and reverse 5′-GCCCAGAGCCTTTTCAT TC-3′. The data from the PCR reaction were normalized against the β-actin expression using the comparative Ct method. The transcripts were quantified in duplicates.

Western blot analysis

Whole-cell or tissue lysates were prepared similarly as previously described[26] from cell lines and primary tumor tissues from four OCCA patients. Twenty-microgram proteins were separated using sodium dodecyl sulfate polyacrylamide gel electrophoresis and blotted on Immobilon P filters (Millipore, Billerica, MA). The following antibodies were used: anti-Cbx7 (1:1,000) (ab21873, Abcam), anti-β-actin (1:2,000) (A5316, Sigma-Aldrich) and anti-PARP (1:1,000) (#9542, Cell Signaling Technology, Beverly, MA). ImmunoStar LD (Wako, Osaka, Japan) was used for chemiluminescence detection.

Cell viability assay

A total of 4,000 cells were transfected with siRNAs in 96-well plates and incubated under 5% CO_2 at 37°C. After 24, 48, 72, and 96 hr, cell viability was assayed by MTS [3-(4,5-dimethylthiazol-2-yl)-5-(3-carboxymethoxyphenyl)-2-(4-sulfophenyl)-2H-tetrazolium] assay using the CellTiter 96 Aqueous One Solution Cell Proliferation Assay kit (Promega, Madison, WI), according to the manufacturer's instructions.

Migration and invasion assay

The assays were performed using 6.5 mm Transwell plates with 8.0 μm pore polycarbonate membrane inserts (Corning Coaster, Rochester, NY). For the invasion assay, the upper surfaces of the filters were coated with 50 μl of matrigel (Becton and Dickenson, Franklin Lakes, NJ). Next, 1×10^5 cells were seeded in the upper chamber in the culture medium without FBS, and the lower chamber contained 10% FBS. The cells were incubated for 24 hr at 37°C in 5% CO_2. After removing the noninvaded or nonmigrated cells, the remaining cells were stained with Giemsa.

Cell cycle analysis

A total of 5×10^5 cells were washed with PBS, fixed with 70% ethanol at −20°C for at least 30 min, washed again with PBS, and incubated with 0.1 mg/ml RNase A solution (QIAGEN) at 37°C for 20 min. The cells were centrifuged, washed again with PBS, and then incubated with 50 μg/ml of propidium iodide (Sigma-Aldrich) on ice for 20 min. The cell cycle profiles were determined using a FACS Calibur

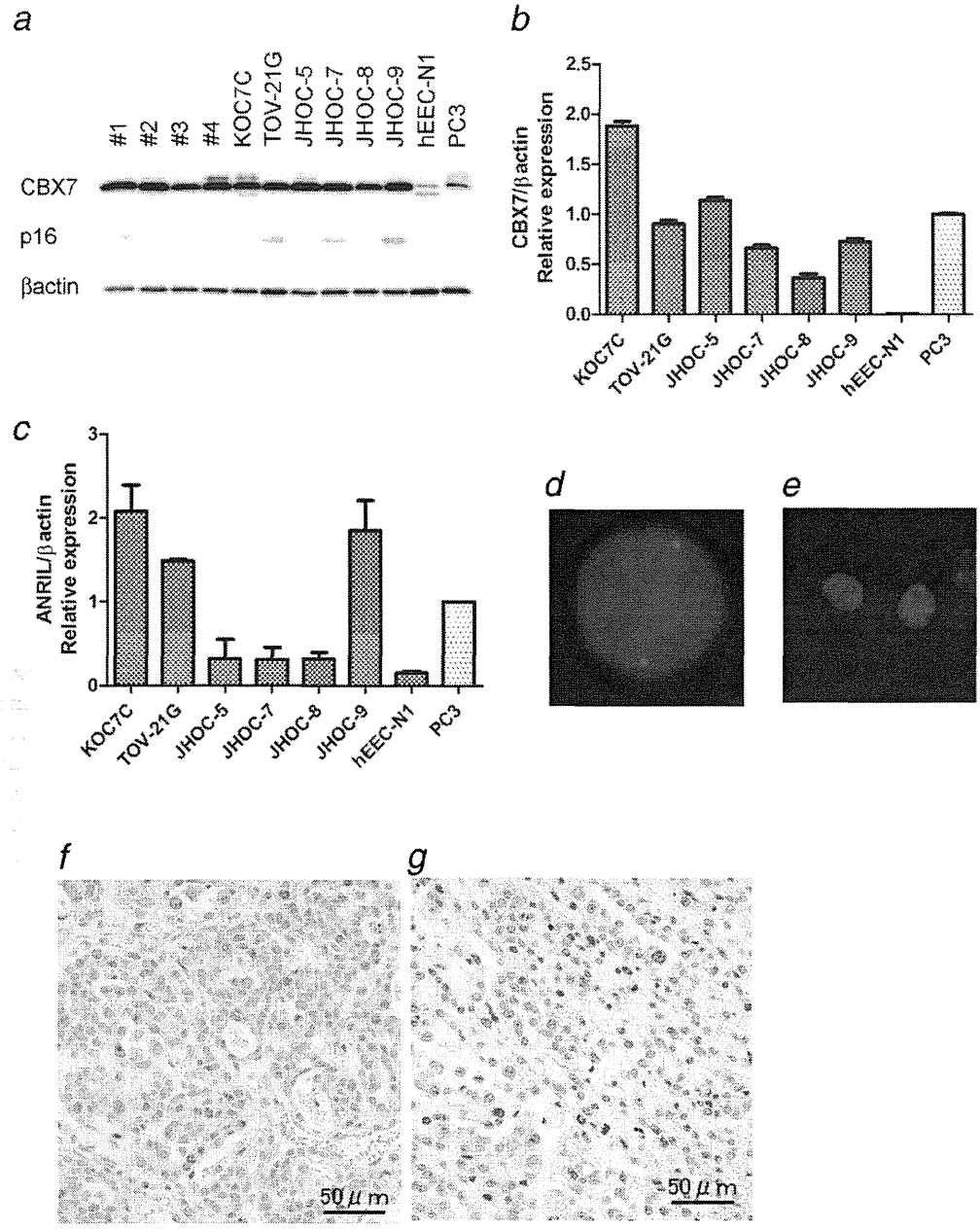

Figure 1. Expression of CBX7 and ANRIL in ovarian clear cell adenocarcinoma (OCCA). (*a–c*) Immunoblotting of four OCCA primary tissue samples (#1,2,3), six OCCA cell lines (KOC-7C, TOV-21G, JHOC-5, -7, -8, -9), a human endometrial epithelial cell line (hEEC-N1) and a positive control prostate cancer cell line, PC3, for detecting CBX7, CDKN2A (p16), and β-actin (*a*). Real-time quantitative reverse transcription PCR analysis using the cells to detect CBX7 (*b*) and ANRIL (*c*). (*d,e*) RNA fluorescence *in situ* hybridization detecting ANRIL (*d*) and fluorescence IHC detecting CBX7 (*e*) in TOV21G cells. Orange signals of both ANRIL and CBX7 are observed in the nuclei of the cells. (*f,g*) Immunohistochemical analysis for CBX7 protein using formalin-fixed paraffin embedded OCCA samples. Intense nuclear staining of the tumor cells is observed (*f*). Negative CBX7 staining (*g*). [Color figure can be viewed in the online issue, which is available at wileyonlinelibrary.com.]

machine (Becton and Dickenson) and analyzed using ModFit LT (Verity Software, Topsham, ME) and CellQuest software (Becton and Dickenson).

Gene expression array analysis

The SurePrint G3 Human Gene Expression 8x60K Microarray (Agilent Technologies, Santa Clara, CA) was used to analyze changes in the mRNA expression levels of the KOC7C and TOV-21G cells after CBX7 knockdown. The microarray targets 27, 958 Entrez Gene RNAs and 7,419 noncoding RNAs. KOC7C and TOV-21G were transfected by siCBX7-1 or negative control siRNA. After 48-hr incubation, total RNA was isolated using the RNeasy Plus Mini Kit (Qiagen). CBX7 knockdown was confirmed by qPCR. Data

Table 1. Multivariate analysis of clinical factors in relation to survival of patients with OCCA

	OS			PFS		
	HR	95% CI	*p*	HR	95% CI	*p*
Age						
≥50 (*vs.* <50)	0.720	0.380–1.952	0.720	0.459	0.203–1.040	0.459
FIGO stage						
II, III, IV (*vs.* I)	3.811	1.652–8.791	0.002	5.467	2.352–12.706	<0.001
CA125 (U/ml)						
≥35 (*vs.* <35)	2.900	0.181–10.282	0.099	2.562	0.827–7.934	0.103
Year of diagnosis						
1997- (*vs.* -1997)	1.186	0.520–2.702	0.685	1.312	0.594–2.897	0.502
CBX7 expression						
Positive (*vs.* negative)	6.767	1.534–29.856	0.012	8.661	1.946–38.559	0.005

HR, hazard ratio; CI, confidence interval.

analysis was performed using GeneSpring GX11.05.1 software (Agilent Technologies).

TdT-mediated dUTP-biotin nick end labeling assay

We performed the TdT-mediated dUTP-biotin nick end labeling (TUNEL) assay to detect apoptotic cells. The cells were transfected with siRNA on chamber slides and cultured in 5% CO_2 at 37°C for 48 hr. We then used the ApopTag Plus Peroxidase *In Situ* Apoptosis Detection Kit (Millipore) following the manufacturer's instructions. Briefly, the cultured cells were fixed with 1% paraformaldehyde and permeabilized using a 2:1 ethanol-acetic acid solution, endogenous peroxidase was quenched using 3% hydrogen peroxide in PBS. After detection, hematoxylin was used as a counterstain. We counted positively stained cells in 10 random fields under 400× magnification and calculated the apoptotic cell ratio.

Statistical analysis

Chi-square tests were used to evaluate the associations between the CBX7 status and clinicopathological factors. The overall survival (OS) was calculated from the date of surgery to the date of the last follow-up or the date of death from OCCA. The progression-free survival (PFS) was calculated from the date of surgery to the date of progression/recurrence or to the date of last follow-up. Survival analyses were performed using the Kaplan–Meier method to estimate the OS and PFS, and statistical significance was determined using the log-rank test. A multivariate analysis was performed using a Cox proportional hazards model. Student's *t*-test (for comparison of the two groups), a one-way ANOVA or a two-way ANOVA (for multiple comparisons) was used to evaluate the numerical data. For all of the statistical analyses, $p < 0.05$ was considered statistically significant.

Results

Expression of CBX7 and ANRIL in OCCA

First, we examined the expression of CBX7 protein and mRNA together with ANRIL RNA in six OCCA cell lines and control by immunoblotting and qPCR (Figs. 1*a*–1*c*), and revealed that both genes, CBX7 and ANRIL, were expressed in all OCCA cell lines. Control human endometrial cells also expressed both genes although smaller in amount. CBX7 was detectable by immunoblotting in the four primary OCCA tissue samples (Fig. 1*a*). Furthermore, we analyzed p16 expression in these cell lines. Because JHOC-5 and JHOC-8 had p16 deletion detected by array comparative genomic hybridization analysis (Supporting Information Figure 1), and JHOC-7 and JHOC-9 had relatively high expression of the p16 protein, we selected KOC-7C and TOV21G for further analyses. We further confirmed the expression of ANRIL and CBX7 protein in the nuclei of both cells by RNA-FISH (Fig. 1*d*) and fluorescence IHC (Fig. 1*e*). Then, we analyzed the expression of CBX7 protein in 81 primary human OCCA tissues by IHC staining. Intense nuclear staining was observed in the positive samples (Fig. 1*f*) in clear contrast with no staining in the negative samples (Fig. 1*g*). Of 81 cases, 64 cases (79%) were CBX7-positive and 17 cases (21%) were CBX7-negative. Next, we examined the association between CBX7 expression and clinical factors. Switching to platinum-taxane chemotherapy which improved OS and PFS in women with ovarian cancer[25] was done in 1997 in our institution. Therefore, we speculated that the year of diagnosis may be associated with prognostic outcome. Furthermore, although most patients were not previously clinically diagnosed as endometriosis, pathological examination of the resected tissue material revealed that the more than 80% had endometriosis (52/64 data available patients, see Supporting Information Table 1). Thus, we added the year of diagnoses and also pathologically diagnosed endometriosis in the analysis. As a result, CBX7 expression was not significantly associated with any of the following factors; patient age, FIGO stage, serum CA125 level, the year of diagnosis, or the presence of endometriosis (Supporting Information Table 1).

CBX7 expression is associated with poor prognosis in patients with OCCA

To further evaluate the role of CBX7 in OCCA, we analyzed the relationship between CBX7 expression and OS and PFS

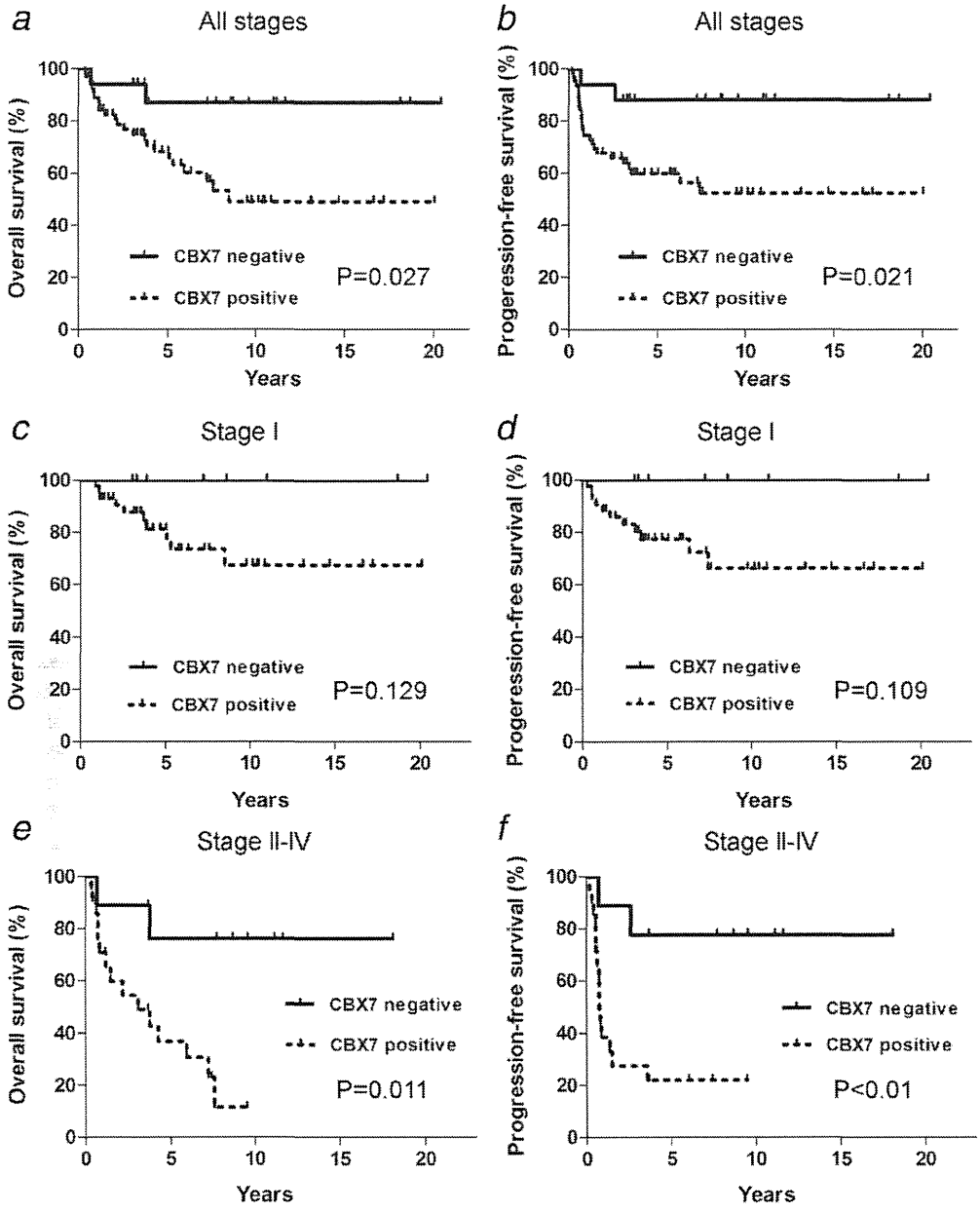

Figure 2. Kaplan–Meier analyses. CBX7 expression is associated with worse OS and PFS in OCCA patients. These Kaplan–Meier survival curves show (*a,b*) OS and PFS in patients with all stages. (*c,d*) OS and PFS in patients with Stage I disease. (*e,f*) OS and PFS in patients with Stages II–IV disease. The solid line indicates the CBX7-negative group, and the dashed line indicates the CBX7-positive group.

using the Kaplan–Meier method together with the log-rank test. The CBX7-positive group had significantly shorter OS ($p = 0.027$, Fig. 2*a*) and PFS ($p = 0.021$, Fig. 2*b*) rates than the CBX7-negative group. However, as most patients with OCCA are diagnosed with Stage I disease (51 cases, 63%), we also analyzed the relationship between CBX7 expression and OS and PFS rates by separating the cases into two groups: the Stage I group and a group consisting of Stages II–IV patients, as categorized at their initial diagnoses. In patients with Stages II–IV disease, the CBX7-positive patients had significantly shorter OS ($p = 0.011$; Fig. 2*e*) and PFS ($p < 0.01$; Fig. 2*f*) rates than the CBX7-negative patients. The CBX7-positive patients tended to have poorer prognoses than the CBX7-negative patients in the Stage I group also, although this difference was not significant (Figs. 2*c* and 2*d*). Similar analysis of endometriosis-positive and negative groups revealed that CBX7 expression was significantly associated with worse OS and PFS rates in the endometriosis-positive group (Supporting Information Figure 2). Endometriosis-negative group also showed a tendency to have worse OS

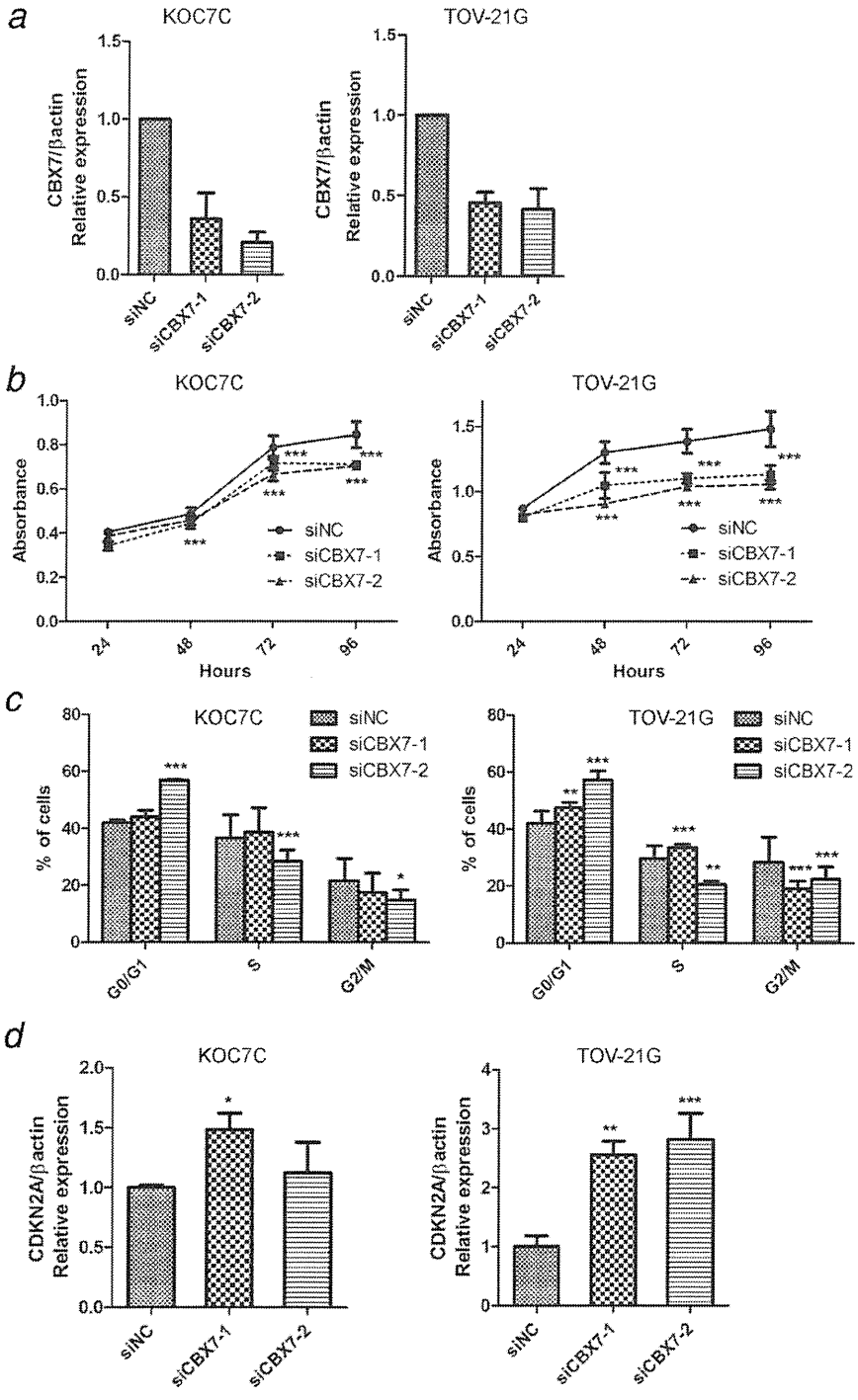

Figure 3. Effects of CBX7 knockdown on OCCA cell lines *in vitro*. After transfection with 2 individual siRNAs (siCBX7-1 and siCBX7-2) or control siRNA in KOC7C and TOV-21G cells, we performed the following experiments. (*a*) The efficacy of two individual siRNAs (siCBX7-1 and siCBX7-2) in KOC7C and TOV-21G measured by quantitative reverse transcriptase-PCR. (*b*) Effects of CBX7 knockdown on cellular viability measured by MTS assay. Hours indicate post-transfection times. (*c*) Cell cycle distribution measured by FACS. (D) Relative expression of CDKN2A (p16) mRNA measured by quantitative reverse transcriptase-PCR compared with control siNC. The means and SD were obtained from three experiments. Statistical analysis was performed to compare CBX7 knockdown and control samples. $*p < 0.05$, $**p < 0.01$, $***p < 0.001$.

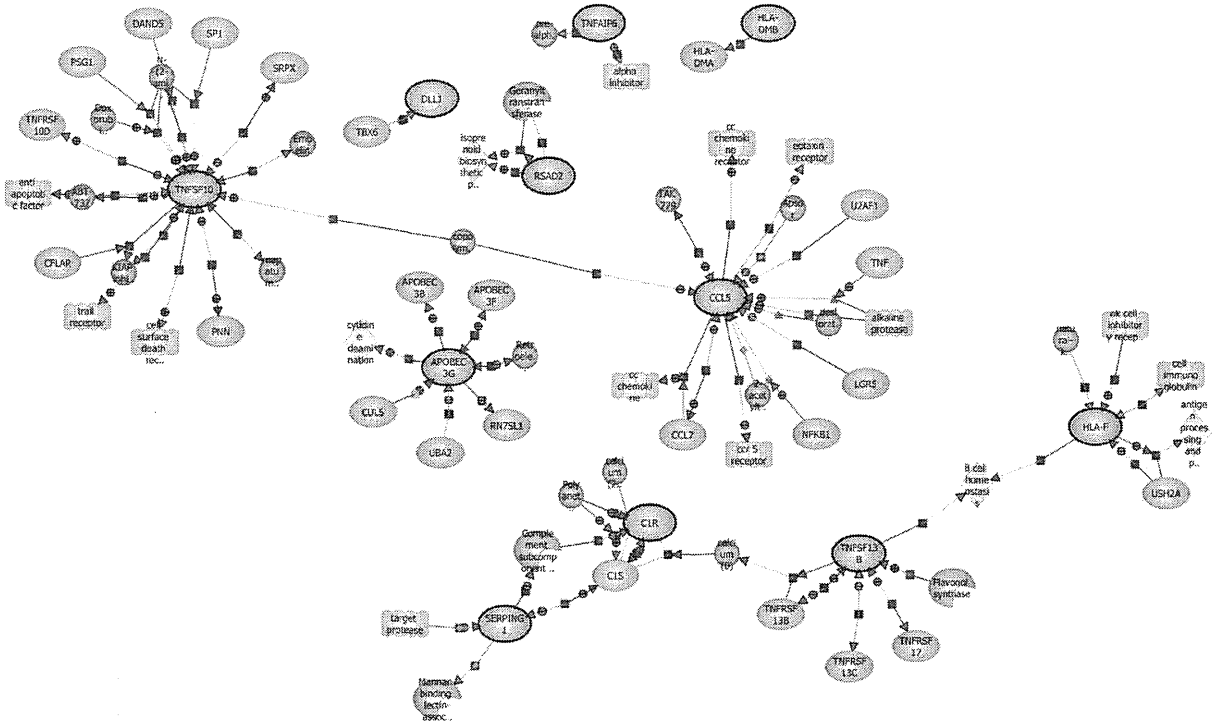

Figure 4. A pathway analysis of 35 genes that had elevated expression levels of more than eightfold compared to CBX7 knockdown groups and the control groups using GeneSpring GX10.02.2 software. [Color figure can be viewed in the online issue, which is available at wileyonlinelibrary.com.]

and PFS related to CBX7 expression, but this relationship was not significant probably due to smaller number of the patients. The presence of endometriosis had no correlation with OS or PFS (Supporting Information Figure 3). Thus, CBX7 seemed to be an independent factor associated with poorer prognosis, and we analyzed the factors that contributed to the prognosis using a multivariate Cox proportional hazards model for confirmation. Statistical results showed that CBX7 expression and FIGO Stages II–VI were associated independently with OS ($p = 0.012$ and $p = 0.002$, respectively) and PFS ($p = 0.005$ and $p < 0.001$, respectively) (Table 1). These results suggest that CBX7 may have a valuable role in OCCA disease progression.

CBX7 knockdown decreases cell viability of human OCCA cells

Because immunohistochemical analysis suggested that CBX7 may contribute to the growth of OCCA, we first examined the effect of CBX7 knockdown on the viability of human OCCA cells. We used two different OCCA cell lines, KOC7C and TOV-21G, and two siRNA constructs against CBX7 to perform the knockdown experiments *in vitro*. The knockdown efficacies of the siRNAs were confirmed 48 hr after transfection by quantitative PCR (Fig. 3*a*) and Western blotting. We assessed cell viability using an MTS assay. CBX7 knockdown significantly inhibited the cell viability of both cell lines, and the decrease in cell viability was maximally 30% (Fig. 3*b*). CBX7 knockdown did not affect cell migration or invasion (data not shown). It has been reported that CBX7 represses the INK4a/ARF locus; therefore, we examined the effect of CBX7 knockdown on p16 expression and cell cycle distribution. CBX7 knockdown significantly induced G0/G1 arrest (Fig. 3*c*) presumably *via* increasing the expression of p16 mRNA (Fig. 3*d*).

CBX7 knockdown induced apoptosis in OCCA cells

From our results, CBX7 was shown to play some role in repressing the CDKN2A gene and the progression of the cell-cycle in the OCCA cells. However, the changes were not dramatic, and because CBX7 expression was clearly related to a poorer prognosis in the OCCA patients, we assumed that CBX7 may help regulate other genes, most likely those related to tumor progression in OCCA. Thus, to examine other possible mechanisms, we compared the gene expression profiles of CBX7 knockdown and control samples from the TOV-21G and KOC7C cell lines using an expression microarray (accession number: GSE47146). We identified 35 genes in which the expression levels were upregulated in the CBX7 knockdown groups in common between both cell lines by more than eightfold compared to the control groups and the statistical values were $p > 0.05$ (Supporting Information Table 2). A pathway analysis indicated that CBX7 negatively

regulates apoptosis-related genes, inflammation-associated genes, such as CCL5, and genes associated with immunological phenotypes, such as HLA-F (Fig. 4). Specifically, TNFSF10, a tumor necrosis factor superfamily 10 member, resided in the center of the apoptosis-related genes (Fig. 4). We confirmed that CBX7 knockdown increased TNFSF10 mRNA expression by qPCR (Fig. 5*a*). To confirm that CBX7 knockdown induced apoptosis in OCCA cells, we performed Western blotting to detect the apoptotic markers along with a TUNEL assay. CBX7 knockdown increased the expression of cleaved PARP proteins (Fig. 5*b*), and the number of apoptotic cells detected by the TUNEL method was significantly increased compared with the control group (Figs. 5*c* and 5*d*). Additionally, we performed DNA content analysis using FACS. The percentage of sub-G1 phase cells (Fig. 5*e*) increased more in the CBX7 knockdown cells than in the control cells.

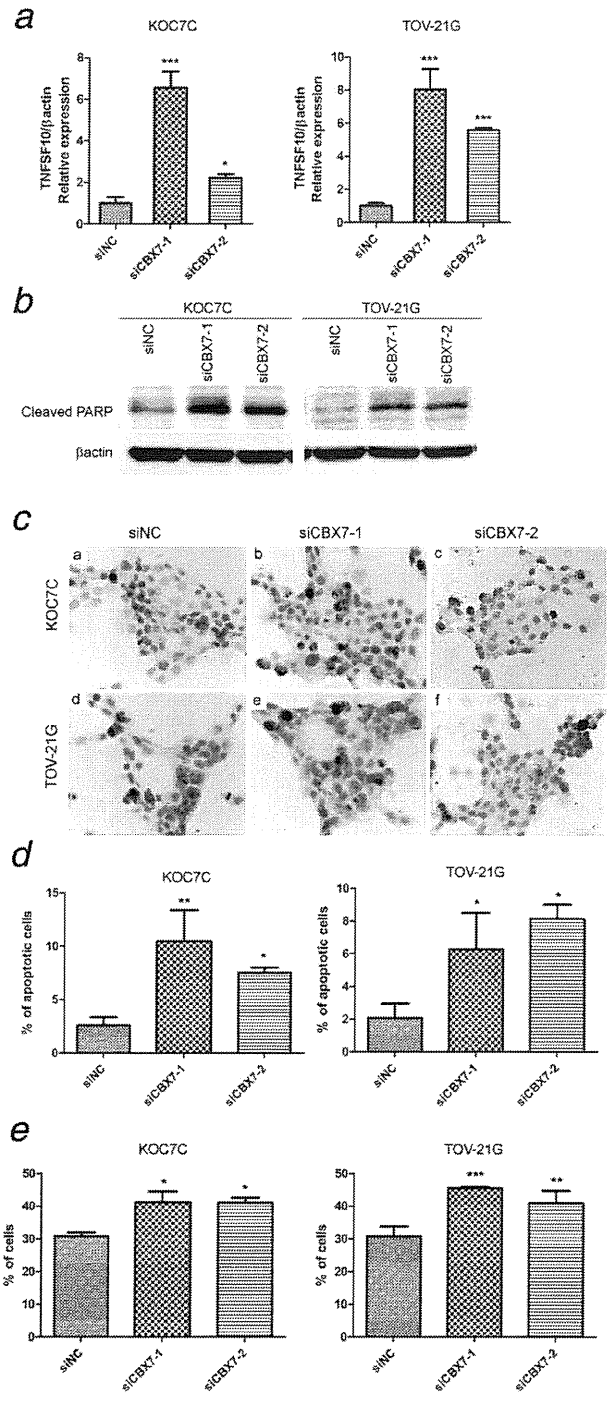

Figure 5. Induction of apoptosis by CBX7 knockdown *in vitro*. After transfection of KOC7C and TOV-21G cells with two individual siRNAs (siCBX7-1 and siCBX7-2) or control siRNA, we performed the following experiments. (*a*) Relative expression of TNFSF10 (TRAIL) mRNA measured by quantitative reverse transcriptase-PCR compared with control. (*b*) Western blotting showed expression of cleaved PARP. (*c*) TUNEL stained cells. (*d*) Percentage of apoptotic cells measured by the TUNEL assay. (*d*) Percentage of sub-G1 cells. siNC indicates the control. Means and SD were obtained from three experiments. Statistical analysis was performed using CBX7 knockdown samples and control samples. $*p < 0.05$, $**p < 0.01$, $***p < 0.001$. [Color figure can be viewed in the online issue, which is available at wileyonlinelibrary.com.]

Discussion

OCCA is frequently associated with endometriosis.[4] Histologically defined endometriosis was also found in more than 80% of our cases (Supporting Information Table 1 and Ref. 6) suggesting that endometriosis has an important role in the development of OCCA. Oxidative stress due to excess iron deposition is assumed as the cause of carcinogenesis.[5,6,27] Genome mutations induced by oxidative stress affects specific genes such as the INK4a region,[28] and although less established, frequent amplification of the MET gene is observed in OCCA,[6] which is common with an oxidative-stress induced animal tumor model.[29] ANRIL is a long noncoding RNA that cooperates with CBX7 to suppress the INK4a/ARF region at chromosome 9. Single-nucleotide polymorphism in the 19th intron of ANRIL was shown to have a strong association with endometriosis.[16] Therefore, we speculated that CBX7 may also have a role in OCCA carcinogenesis and progression. As a result, we demonstrated for the first time that CBX7 expression was associated with poorer prognosis in OCCA patients.

CBX7 was initially identified as a factor involved in overcoming cellular senescence and increasing cellular lifespan.[11] CBX7 is one of the PcG proteins, a family that also includes BMI1 and EZH2, and it is a component of PRC1.[9] Most PcG proteins have been known to have strong associations with cancer development, and some of these proteins have also been related to stem cell regulation.[11] EZH2 was recently shown as an tumorigenic independently of PRC,[30] and it is acceptable that other PcG proteins such as CBX7 may also have a distinct oncogenic role. PcG proteins have hundreds of target genes in mammals, and mammalian polycomb

responsive elements are not yet defined.[9] It has been shown that CBX7 plays a critical role in the lymphomagenesis of follicular lymphoma,[13] however, controversial studies have also shown that CBX7 positively regulates E-cadherin expression, thus acting as a tumor suppressor in thyroid cancer.[18,20] CBX7 protein expression loss has also been observed in colon and pancreatic cancer patients with aggressive tumors.[17,31] Most recently, CBX7 knockout mice were shown to have a tumorigenic phenotype that was associated with liver and lung carcinogenesis, and a new role for CBX7, downregulating cyclin E1, was reported.[21] Thus, the precise role of CBX7 in cancer development or progression may be cell-type specific, and in this report, we show for the first time that CBX7 has a progressive role in malignant behavior of OCCA.

It has been reported that PRC1 including CBX7 suppresses the INK4A locus together with ANRIL, which in turn leads to a reduction in the levels of tumor suppressor proteins such as p16 and p14ARF in prostate cancer cells.[12] Because we mainly used formalin-fixed paraffin-embedded tissue for the analyses in this study, we could not determine the relative rate of ANRIL expression in each sample. However, in this study, ANRIL expression was observed in six OCCA cell lines shown by qPCR and also expressed in the nuclei of two cell lines by RNA-FISH. Thus, consistent with previous reports, our data also showed that CBX7, possibly together with ANRIL, could repress the INK4a/ARF locus in the OCCA cells. However, relatively high expression of p16 was detected by immunoblotting in two OCCA cell lines other than KOC7C and TOV21G (Fig. 1*a*). Relative expression increases shown by qPCR in p16 (induced by CBX7 knockdown) were two- to threefold the maximum levels; while this change was not large, it was significant (Fig. 3*d*). On the contrary, G1 arrest induced by CBX7 knockdown was nonsignificant (Fig. 3*c*) in KOC7C cells. We attempted to increase the rate of G1 arrest by ubiquitously demethylating the promotor areas including the p16 promotor by adding 5-azacythidine to the culture medium, and as a result, p16 expression was slightly increased in KOC-7C cells; however, together with CBX7 knockdown, no significant increase in either p16 expression or G1 arrest was observed in these cells (Supporting Information Figure 4). Therefore, although we could not deny the possibility that ANRIL expression level was critical in downregulating the INK4a/ARF locus, but at least, in part, the expression levels of p16 significantly enlarged, and CBX7 knockdown itself was confirmed at both mRNA and the protein level, we considered that there may be other genes that are either directly or indirectly regulated by CBX7.

Interestingly, pathway analysis of the microarray data elucidated that a group of apoptosis-related genes were upregulated by CBX7 knockdown, and TNSF10 was positioned in the center of this group. TNFSF10 is also known as TRAIL (tumor necrosis factor-related apoptosis-inducing ligand). TRAIL induces apoptosis by binding to TRAIL-R1 (also known as DR4) and TRAIL-R2 (also known as DR5), and its binding triggers caspase-8 and caspase-3 activations. We further confirmed that CBX7 knockdown significantly induced apoptosis in both cell lines, with two different siRNAs for each one. TRAIL is an important inducer of apoptosis, but the precise mechanism for the regulation of its expression is still unknown.[32] In our study, CBX7 was shown to play a role in inducing the expression of TRAIL and related apoptotic factors. Whether CBX7 together with PRCs directly suppresses any of these molecules remains to be elucidated. TRAIL is an important factor for apoptosis induction in cancer cells, and studies are ongoing to seek novel therapeutic agents, such as TRAIL, and agonistic antibodies against TRAIL receptors are promising new antitumor agents.[33] Recently, however, resistance to TRAIL agonists has been found in some human cancers. This finding suggests that therapy using the TRAIL pathway may be cell-type specific.[34] Our results suggest that TRAIL pathway may be a novel target for CBX7, which may have a biological role in OCCA carcinogenesis and progression. Therapeutic agents utilizing the TRAIL pathway may be particularly effective in OCCA.

Acknowledgement

We thank Ms. Y Tanaka and Mr. N Misawa for their excellent technical assistance.

References

1. Japanese Gynecological Committee. Annual report on Japanese gynecologic cancer of 2010. *Acta Obstet Gynaecol Jpn* 2012:1071.
2. Del Carmen MG, Birrer M, Schorge JO. Clear cell carcinoma of the ovary: a review of the literature. *Gynecol Oncol* 2012;126:481–90.
3. Kennedy AW, Biscotti CV, Hart WR, et al. Ovarian clear cell adenocarcinoma. *Gynecol Oncol* 1989;32:342–9.
4. Pearce CL, Templeman C, Rossing MA, et al. Association between endometriosis and risk of histological subtypes of ovarian cancer: a pooled analysis of case-control studies. *Lancet Oncol* 2012;13:385–94.
5. Yamaguchi K, Mandai M, Toyokuni S, et al. Contents of endometriotic cysts, especially the high concentration of free iron, are a possible cause of carcinogenesis in the cysts through the iron-induced persistent oxidative stress. *Clin Cancer Res* 2008;14:32–40.
6. Yamashita Y, Akatsuka S, Shinjo K, et al. Met is the most frequently amplified gene in endometriosis-associated ovarian clear cell adenocarcinoma and correlates with worsened prognosis. *PloS One* 2013;8:e57724.
7. Mackay HJ, Brady MF, Oza AM, et al. Prognostic relevance of uncommon ovarian histology in women with stage III/IV epithelial ovarian cancer. *Int J Gynecol Cancer* 2010;20:945–52.
8. Sugiyama T, Kamura T, Kigawa J, et al. Clinical characteristics of clear cell carcinoma of the ovary—a distinct histologic type with poor prognosis and resistance to platinum-based chemotherapy. *Cancer* 2000;88:2584–9.
9. Simon JA, Kingston RE. Mechanisms of Polycomb gene silencing: knowns and unknowns. *Nat Rev Mol Cell Biol* 2009;10:697–708.
10. Richly H, Aloia L, Di Croce L. Roles of the Polycomb group proteins in stem cells and cancer. *Cell Death Dis* 2011;2:e204.
11. Gil J, Bernard D, Martinez D, et al. Polycomb CBX7 has a unifying role in cellular lifespan. *Nat Cell Biol* 2004;6:67–72.
12. Bernard D, Martinez-Leal JF, Rizzo S, et al. CBX7 controls the growth of normal and tumor-derived prostate cells by repressing the Ink4a/Arf locus. *Oncogene* 2005;24:5543–51.

13. Scott CL, Gil J, Hernando E, et al. Role of the chromobox protein CBX7 in lymphomagenesis. *Proc Nat Acad Sci USA* 2007;104:5389–94.
14. Zhang X-W, Zhang L, Qin W, et al. Oncogenic role of the chromobox protein CBX7 in gastric cancer. *J Exp Clin Cancer Res* 2010;29:114.
15. Yap KL, Li S, Munoz-Cabello AM, et al. Molecular interplay of the noncoding RNA ANRIL and methylated histone H3 lysine 27 by Polycomb CBX7 in transcriptional silencing of INK4a. *Mol Cell* 2010;38:662–74.
16. Uno S, Zembutsu H, Hirasawa A, et al. A genome-wide association study identifies genetic variants in the CDKN2BAS locus associated with endometriosis in Japanese. *Nat Genet* 2010;42: U70–U88.
17. Karamitopoulou E, Pallante P, Zlobec I, et al. Loss of the CBX7 protein expression correlates with a more aggressive phenotype in pancreatic cancer. *Eur J Cancer* 2010;46:1438–44.
18. Pallante P, Federico A, Berlingieri MT, et al. Loss of the CBX7 gene expression correlates with a highly malignant phenotype in thyroid cancer. *Cancer Res* 2008;68:6770–8.
19. Forzati F, Federico A, Pallante P, et al. Tumor suppressor activity of CBX7 in lung carcinogenesis. *Cell Cycle* 2012;11:1888–91.
20. Federico A, Pallante P, Bianco M, et al. Chromobox protein homologue 7 protein, with decreased expression in human carcinomas, positively regulates E-cadherin expression by interacting with the histone deacetylase 2 protein. *Cancer Res* 2009;69:7079–87.
21. Forzati F, Federico A, Pallante P, et al. CBX7 is a tumor suppressor in mice and humans. *J Clin Invest* 2012;122:612–23.
22. Krenke BE, Tereba A, Anderson SJ, et al. Validation of a 16-locus fluorescent multiplex system. *J Forensic Sci* 2002;47:773–85.
23. Kobayashi H, Yamashita Y, Iwase A, et al. The ferroimmunomodulatory role of ectopic endometriotic stromal cells in ovarian endometriosis. *Fertil Steril* 2012;98:415–22.
24. Yamashita Y, Kajiura D, Tang L, et al. XCR1 expression and biased VH gene usage are distinct features of diffuse large B-cell lymphoma initially manifesting in the bone marrow. *Am J Clin Pathol* 2011;135:556–64.
25. Yamashita Y, Tsurumi T, Mori N, et al. Immortalization of Epstein-Barr virus-negative human B lymphocytes with minimal chromosomal instability. *Pathol Int* 2006;56:659–67.
26. McGuire WP, Hoskins WJ, Brady MF, et al. Cyclophosphamide and cisplatin compared with paclitaxel and cisplatin in patients with stage III and stage IV ovarian cancer. *N Engl J Med* 1996; 334:1–6.
27. Yamaguchi K, Mandai M, Oura T, et al. Identification of an ovarian clear cell carcinoma gene signature that reflects inherent disease biology and the carcinogenic processes. *Oncogene* 29: 1741–52.
28. Toyokuni S. Molecular mechanisms of oxidative stress-induced carcinogenesis: from epidemiology to oxygenomics. *IUBMB life* 2008;60:441–7.
29. Akatsuka S, Yamashita Y, Ohara H, et al. Fenton reaction induced cancer in wild type rats recapitulates genomic alterations observed in human cancer. *PloS One* 2012;7:e43403.
30. Xu K, Wu ZJ, Groner AC, et al. EZH2 oncogenic activity in castration-resistant prostate cancer cells is Polycomb-independent. *Science* 2012;338: 1465–9.
31. Pallante P, Terracciano L, Carafa V, et al. The loss of the CBX7 gene expression represents an adverse prognostic marker for survival of colon carcinoma patients. *Eur J Cancer* 2010;46:2304–13.
32. Allen JE, El-Deiry WS. Regulation of the human TRAIL gene. *Cancer Biol Ther* 13:1143–51.
33. Johnstone RW, Frew AJ, Smyth MJ. The TRAIL apoptotic pathway in cancer onset, progression and therapy. *Nat Rev Cancer* 2008;8:782–98.
34. Dimberg LY, Anderson CK, Camidge R, et al. On the TRAIL to successful cancer therapy?. Predicting and counteracting resistance against TRAIL-based therapeutics. *Oncogene* 2012;32: 1341–50.

Carcinogenesis vol.35 no.1 pp.164–172, 2014
doi:10.1093/carcin/bgt267
Advance Access publication July 19, 2013

Cancer-promoting role of adipocytes in asbestos-induced mesothelial carcinogenesis through dysregulated adipocytokine production

Shan Hwu Chew[1], Yasumasa Okazaki[1], Hirotaka Nagai[1,2], Nobuaki Misawa[1], Shinya Akatsuka[1], Kyoko Yamashita[1], Li Jiang[1], Yoriko Yamashita[1], Michio Noguchi[3], Kiminori Hosoda[3,4], Yoshitaka Sekido[5], Takashi Takahashi[6] and Shinya Toyokuni[1,*]

[1]Department of Pathology and Biological Responses, Nagoya University Graduate School of Medicine, Nagoya 466-8550, Japan, [2]Department of Pathology and Biology of Diseases, [3]Department of Endocrinology and Metabolism and [4]Faculty of Human Health Science, Kyoto University Graduate School of Medicine, Kyoto 606-8315, Japan, [5]Division of Molecular Oncology, Aichi Cancer Center Research Institute, Nagoya 464-8681, Japan and [6]Department of Molecular Carcinogenesis, Nagoya University Graduate School of Medicine, Nagoya 466-8550, Japan

*To whom correspondence should be addressed. Tel: +81 52 744 2086; Fax: +81 52 744 2091;
Email: toyokuni@med.nagoya-u.ac.jp

Like many other human cancers, the development of malignant mesothelioma is closely associated with a chronic inflammatory condition. Both macrophages and mesothelial cells play crucial roles in the inflammatory response caused by asbestos exposure. Here, we show that adipocytes can also contribute to asbestos-induced inflammation through dysregulated adipocytokine production. 3T3-L1 preadipocytes were differentiated into mature adipocytes prior to use. These cells took up asbestos fibers (chrysotile, crocidolite and amosite) but were more resistant to asbestos-induced injury than macrophages and mesothelial cells. Expression microarray analysis followed by reverse transcription–PCR revealed that adipocytes respond directly to asbestos exposure with an increased production of proinflammatory adipocytokines [e.g. monocyte chemoattractant protein-1 (MCP-1)], whereas the production of anti-inflammatory adipocytokines (e.g. adiponectin) is suppressed. This was confirmed in epididymal fat pad of mice after intraperitoneal injection of asbestos fibers. Such dysregulated adipocytokine production favors the establishment of a proinflammatory environment. Furthermore, MCP-1 marginally promoted the growth of MeT-5A mesothelial cells and significantly enhanced the wound healing of Y-MESO-8A and Y-MESO-8D human mesothelioma cells. Our results suggest that increased levels of adipocytokines, such as MCP-1, can potentially contribute to the promotion of mesothelial carcinogenesis through the enhanced recruitment of inflammatory cells as well as a direct growth and migration stimulatory effect on mesothelial and mesothelioma cells. Taken together, our findings support a potential cancer-promoting role of adipocytes in asbestos-induced mesothelial carcinogenesis.

Introduction

Malignant mesothelioma, which arises from the mesothelial cells lining the pleural, peritoneal and pericardial cavity, is closely associated with exposure to asbestos fibers. The first convincing evidence of an etiologic relationship between asbestos fibers and malignant mesothelioma emerged in 1960 (1). Since then, there has been considerable interest in unraveling the mechanisms underlying asbestos-induced mesothelial carcinogenesis. Macrophages were the first to receive great attention, as asbestos exposure is often associated with a chronic granulomatous inflammatory response. Several groups reported the activation of macrophages by asbestos fibers, and they showed that asbestos fibers were able to induce macrophages to release a multitude of factors, such as lysosomal enzymes, cytokines, plasminogen activators and reactive oxygen species (2–4), which collectively contribute to chronic inflammation. Subsequent studies revealed a direct interaction between asbestos fibers and mesothelial cells, and asbestos fibers were shown to be able to activate certain signaling cascades within mesothelial cells. This activation might be critical for mesothelial transformation (5–8). In addition, mesothelial cells themselves also play a role in the inflammatory response. Mesothelial cells are particularly sensitive to the cytotoxic effect of asbestos fibers. Yang *et al.* (9) termed the process of asbestos-induced mesothelial cell death as 'programmed necrosis', and they reported that during this process, there was an extensive release of high-mobility group box 1 into the extracellular space, which then initiated a chronic inflammatory response by inducing the macrophages to release tumor necrosis factor-α. Together, this evidence strongly supports the vital role of chronic inflammation in asbestos carcinogenicity.

To establish an animal model of mesothelioma, asbestos fibers are usually injected into the pleural or peritoneal cavity (10–12). According to some previous reports, the peritoneal cavity appeared to be more sensitive to the effect of asbestos fibers compared with the pleural cavity, i.e. malignant mesothelioma developed more frequently and rapidly in the peritoneal cavity following asbestos injection (13,14). We speculated that this finding might be related to the abundance of adipose tissue in the peritoneal cavity. A substantial body of recent evidence has revealed the role of adipose tissue in inflammation, particularly in obesity-related inflammation (15–17). This inflammatory response in the adipose tissue of obese individuals is linked to the development of type 2 diabetes mellitus.

Adipose tissue is now recognized as an endocrine organ that is capable of secreting a wide variety of biologically active peptides collectively known as adipocytokines [e.g. monocyte chemoattractant protein-1 (MCP-1), interleukin-6 (IL-6), leptin, adiponectin, plasminogen activator inhibitor-1 (PAI-1), resistin and visfatin]. Evidence from numerous epidemiologic studies has revealed an increased risk of cancer development in obese individuals, further supporting a cancer-promoting role of adipose tissue (18–21). Obesity has been defined as a low-grade chronic inflammatory condition. Many groups have reported that the dysregulated endocrine function of adipose tissue underlies this obesity-related inflammation (22–25). Dysregulation of adipose tissue generally results in the enhanced production of proinflammatory adipocytokines and suppression of anti-inflammatory adipocytokines.

Some previous studies have demonstrated the ability of adipocytes to perform phagocytosis in a macrophage-like manner (26,27). A direct interaction between asbestos fibers and adipocytes involving fiber internalization is thus very likely to take place. We hypothesized that this interaction can trigger off an inflammatory response in adipocytes which occurs through dysregulation of adipocytokine production, as in obesity. Due to the close anatomic proximity between adipocytes and mesothelial cells, altered levels of adipocytokines can potentially affect mesothelial cells in a paracrine manner. We performed this study to evaluate the potential involvement of adipose tissue as a cancer promoter in asbestos-induced carcinogenesis through its ability to aggravate the inflammatory response.

Abbreviations: Ccl, chemokine C-C motif ligand; FBS, fetal bovine serum; IL-6, interleukin-6; MCP-1, monocyte chemoattractant protein-1; mRNA, messenger RNA; MTT, thiazolyl blue tetrazolium bromide; NT-tngl, tangled carbon nanotubes; PAI-1, plasminogen activator inhibitor-1; Prl2c5, prolactin family 2, subfamily c, member 5; RT–PCR, reverse transcription–PCR.

Materials and methods

Materials

Three types of Union for International Cancer Control asbestos fibers (chrysotile A, crocidolite and amosite) were suspended in physiological saline. Tangled carbon nanotubes (NT-tngl, diameter = 15 nm; VGCF-X, Showa Denko, Tokyo, Japan) were suspended in physiological saline containing 0.5% bovine serum albumin. The 3T3-L1 preadipocyte cell line was a kind gift from Dr M.N. and Prof. K.H. (Kyoto University, Kyoto, Japan). MeT-5A and RAW264.7 cell lines were obtained from American Type Culture Collection (Manassas, VA). Y-MESO-8A and Y-MESO-8D cell lines were kindly provided by Prof. Y.S. (Aichi Cancer Centre Research Institute, Nagoya, Japan). These two human mesothelioma cell lines were established from the same Japanese patient with biphasic-like characteristics of malignant pleural mesothelioma and they showed epithelial and sarcomatous phenotypes, respectively, in cell culture (28). Recombinant human MCP-1 was purchased from PeproTech (Rocky Hill, NJ). Thiazolyl blue tetrazolium bromide (MTT) was purchased from Sigma (St Louis, MO). Dimethyl sulfoxide was purchased from Wako (Osaka, Japan).

Cell culture

3T3-L1 preadipocytes were maintained in Dulbecco's modified Eagle's medium supplemented with 10% calf serum and antibiotics. The differentiation of these preadipocytes into mature adipocytes was induced with Dulbecco's modified Eagle's medium supplemented with 10% fetal bovine serum (FBS), 0.5 mM 3-isobutyl-1-methyl-xanthine, 0.25 μM dexamethasone and 1 μg/ml insulin. Mature adipocytes were used for experiments within 10–14 days after the induction of differentiation. The RAW264.7 macrophage cell line was maintained in Dulbecco's modified Eagle's medium supplemented with 10% FBS and antibiotics. MeT-5A, a human mesothelial cell line immortalized through transfection with the pRSV-T plasmid (an SV40 ori-construct containing the SV40 early region and the Rous sarcoma virus long terminal repeat), was maintained in M199 medium supplemented with 10% FBS, 10 ng/ml epidermal growth factor, 870 nM insulin, 400 nM hydrocortisone, 0.3% (vol/vol) trace element B and antibiotics. Y-MESO-8A and Y-MESO-8D cell lines were maintained in RPMI 1640 medium supplemented with 10% FBS and antibiotics. All the cells were cultured in a humidified incubator with 5% CO_2 at 37°C.

Experimental animals

For animal experiments, 8-week-old male ddY mice (Japan SLC, Hamamatsu, Shizuoka, Japan) were used. The animals were housed in a specific pathogen-free animal facility with 12 h light/12 h dark cycle and allowed free access to food (CE-2, CLEA Japan, Tokyo, Japan) and water. These mice were subjected to a single intraperitoneal injection of 2.5 mg of asbestos fibers and killed after 3 days via cervical dislocation. Physiological saline (0.9%) was injected as a control. After killing, the epididymal fat pad was harvested; half of it was fixed in 10% phosphate-buffered formalin for histological analysis, whereas the other half was snap-frozen in liquid nitrogen and kept at −80°C until further use. The animal experiment was approved by the Animal Experiment Committee of the Nagoya University Graduate School of Medicine.

Oil Red O staining of adipocytes

Adipocyte maturation from the preadipocyte cell line was confirmed by staining the lipid droplets that accumulated in the cytoplasm of adipocytes during maturation using the Oil Red O staining method. After washing the mature adipocytes with phosphate-buffered saline, the cells were fixed with 10% phosphate-buffered formalin for 2 h. After another washing step, Oil Red O solution was added, and the cells were incubated at 37°C for 5 min. Images were acquired using a Nikon Eclipse TS-100 microscope (Nikon, Tokyo, Japan).

Fiber uptake by adipocytes

The uptake of asbestos fibers by adipocytes was analyzed by both light microscopy and transmission electron microscopy. Cultured adipocytes were exposed to 10 μg/cm^2 of asbestos fibers, and 24 h later, the cells were harvested by trypsinization and centrifuged to generate a cell pellet. For light microscopy, cell block was prepared by fixing the cells with 10% phosphate-buffered formalin and subsequently processed into a paraffin-embedded cell block. Sections of 4 μm were stained with Kernechtrot staining and viewed under ×100 magnification using a BZ-9000 microscope (Keyence, Osaka, Japan) to detect fibers inside the cells. For electron microscopy, cells were fixed with phosphate buffer containing 2.5% glutaraldehyde and 2% paraformaldehyde, followed by fixation with 1% osmium tetroxide. The cells were then embedded in Epon resin and cut into 80 nm ultrathin sections with diamond knife. After staining with uranyl acetate and lead citrate, detection of fibers inside the cells was performed using JEM-1400EX transmission electron microscope (JEOL, Tokyo, Japan).

Cell viability assay

The cytotoxicity of asbestos fibers on adipocytes, MeT-5A and RAW264.7 macrophages was measured using a CellTiter-Glo Luminescent Cell Viability Assay (Promega, Madison, WI). Asbestos fibers were added to the cells at a concentration of 10 μg/cm^2. After 72 h of incubation, the number of viable cells was evaluated via the addition of the CellTiter-Glo Luminescent Cell Viability Assay reagent followed by chemiluminescence measurement using a PowerScan4 plate reader (DS Pharma Biomedical, Osaka, Japan).

Microarray-based gene expression analysis

Microarray analysis was performed using an Agilent SurePrint G3 Mouse GE 8x60K Microarray slide and Agilent's Low Input Quick Amp Labeling Kit (Agilent Technologies, Santa Clara, CA) according to Agilent's One-Color Microarray-Based Gene Expression Analysis protocol. In total, 200 ng of total RNA extracted from adipocytes exposed to asbestos fibers under the conditions stated above was used as the initial material. Amplified cRNA was labeled with Cy3-CTP. Hybridization was performed by placing the slide in a hybridization oven equipped with a rotator and set at 65°C for 17 h. After hybridization, the microarray slide was washed with GE Wash Buffer and scanned, and data were analyzed using GeneSpring GX 10.02.2 software (Agilent Technologies).

Quantitative real-time reverse transcription–PCR

Total RNA was isolated from the differentiated adipocyte cell line or adipose tissue using the RNeasy Lipid Tissue Mini Kit (Qiagen, Valencia, CA). Total RNA was then reversed transcribed into complementary DNA using the SuperScript III First-Strand Synthesis Kit (Invitrogen, Grand Island, NY). Gene expression levels were quantitatively measured using the Platinum SYBR Green qPCR SuperMix-UDG kit (Invitrogen) and analyzed with an Applied Biosystems Model 7300 Real Time PCR System (Applied Biosystems, Foster City, CA). The β-actin level was used to normalize the messenger RNA (mRNA) level of all genes examined. The primer sequences used were as follows: mouse IL-6, forward, 5′-CTTCTTGGGACTGATGCTGG-3′, reverse, 5′-CAGAATTGCCATTGCACAAC-3′ (product size 185 bp); mouse β-actin, forward, 5′-ACATCCCCCAAAGTTCTACAAA-3′, reverse, 5′-TGAGGGACTTCCTGTAACCACT-3′ (product size 132 bp); mouse adiponectin, forward, 5′-GCAGGCATCCCAGGACATCC-3′, reverse, 5′-TCCTTTCCTGCCAGGGGTTC-3′ (product size 186 bp); mouse MCP-1, forward, 5′-CAGTTAACGCCCCACTCACC-3′, reverse, 5′-TCCTTCTTGG GGTCAGCACA-3′ (product size 163 bp); mouse prolactin family 2, subfamily c, member 5 (Prl2c5), forward, 5′-AACAAGGAACAAGCCAGGCACA-3′, reverse, 5′-ACCCCGTTCTGGACTGCGTT-3′ (product size 188 bp); mouse leptin, forward, 5′-CCAGCAGCTGCAAGGTGCAAGA-3′, reverse, 5′-CCCTCTGCTTGGCGGATACCGA-3′ (product size 214 bp) and mouse PAI-1, forward, 5′-ATGTGCACCTCTCCGCCCTCA-3′, reverse, 5′-GCTGCTCTTGGTCGGAAAGACTTG-3′ (product size 213 bp).

MCP-1 enzyme-linked immunosorbent assay

Differentiated adipocytes in a 6-well plate were exposed to different types of asbestos fibers and NT-tngl at 10 μg/cm^2 for 72 h. The cell culture medium was then collected, and the concentration of MCP-1 secreted by adipocytes into the culture medium was measured using the Quantikine Mouse JE/MCP-1 Immunoassay Kit (R&D Systems, Minneapolis, MN). The immunoassay was performed according to the manufacturer's instructions.

Immunohistochemistry

Paraffin-embedded tissue sections were deparaffinized and rehydrated. Antigen retrieval was performed by heating the sections with microwave using 10 mM citrate buffer, pH 6.0. Endogenous peroxidase was inhibited by incubating the sections with 0.3% hydrogen peroxide in methanol for 30 min. Tissue sections were then blocked with normal goat serum and incubated with rabbit polyclonal primary antibody against mouse MCP-1 (ab7202, abcam, Tokyo, Japan) or IL-6 (ab6672; abcam). After washing with phosphate-buffered saline, sections were incubated with biotinylated goat anti-rabbit immunoglobulin G secondary antibody. Detection of antigen–antibody complexes was performed by incubating the sections with horseradish peroxidase-conjugated streptavidin followed by 3,3′-diaminobenzidine. Images were acquired using BZ 9000 microscope.

Measurement of adipocyte size

Images of epididymal adipose tissue sections were acquired using BZ 9000 microscope at ×40 magnification. Ten random fields were taken for each section from five animals per group. Cell surface area was measured using ImageJ software (NIH, Bethesda, MD).

Transwell migration assay

Cell culture inserts and 24-well companion tissue culture plates from BD Falcon (Franklin Lakes, NJ) were used for transwell migration assay. The

cell culture insert contains a porous membrane with an 8 μm pore size. RAW264.7 macrophages were seeded into the insert at a density of 2 × 10^5 cells/insert. Conditioned medium collected from adipocytes that were treated or untreated with asbestos fibers was added to the lower chamber of the 24-well tissue culture plate. The plate was incubated for 24 h, followed by staining of the migrated cells with May–Grunwald's and Giemsa stains. Images were acquired in 10 random fields, and the number of migrated cells was counted.

MTT cell proliferation assay

MeT-5A cells were seeded into a 96-well tissue culture plate at a density of 5 × 10^3 cells/well. These cells were serum starved for 24 h before being treated with recombinant human MCP-1 at a concentration of 100 and 500 ng/ml. After 72 h of treatment, cell proliferation was measured using MTT. The MTT compound was dissolved in phosphate-buffered saline at a concentration of 5 mg/ml, and 20 μl was then added to each well. Cells were incubated with MTT for 4 h to allow the reduction of MTT into purple formazan. Culture

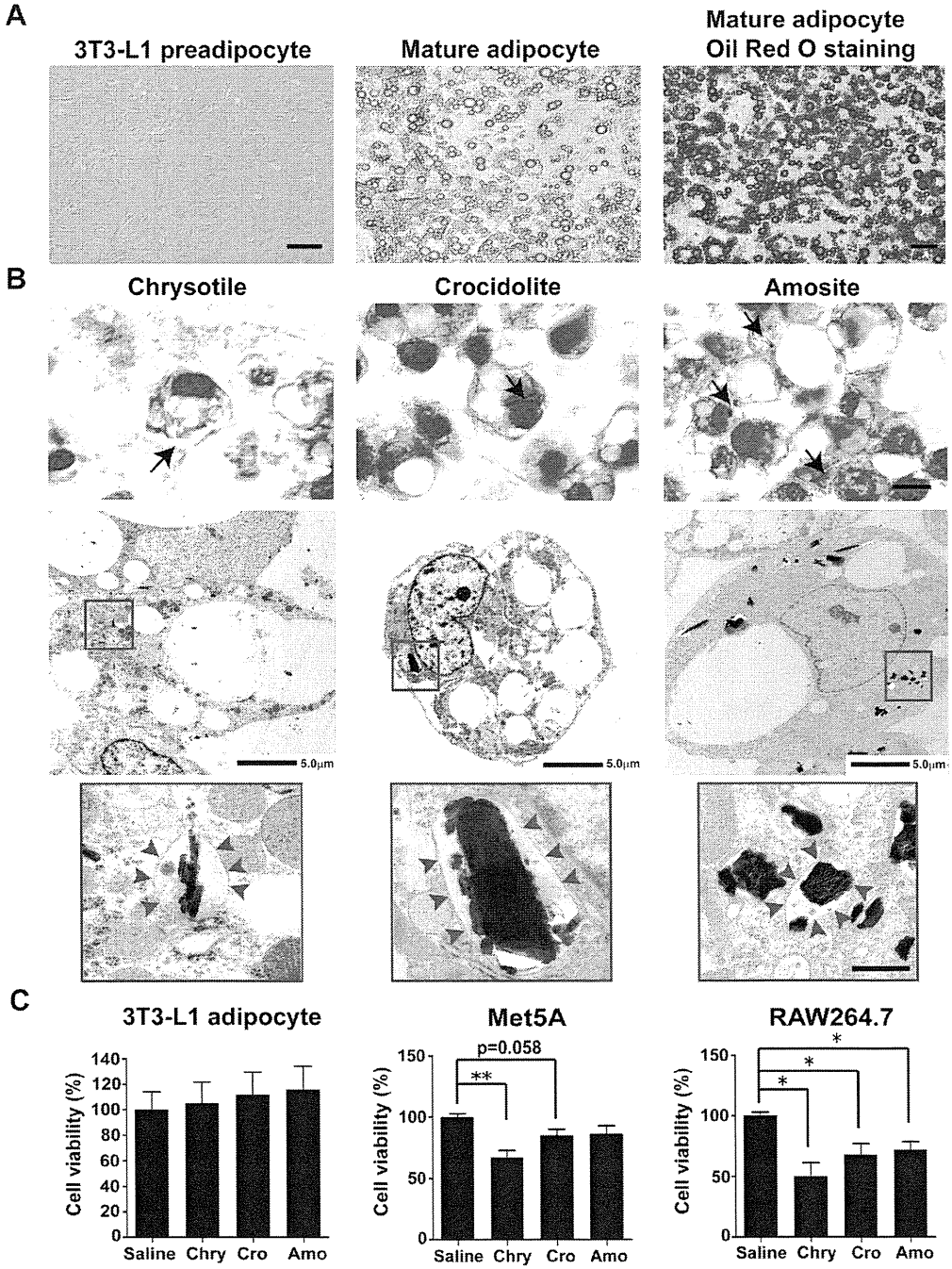

Fig. 1. Cultured adipocytes take up asbestos fibers but are resistant to their cytotoxic effect. (**A**) The 3T3-L1 preadipocyte cell line (left panel) was differentiated into mature adipocytes (middle panel) according to the standard differentiation protocol. Lipid droplets that accumulated in the mature adipocytes were stained by Oil Red O staining (right panel). Scale bars: left panel, 100 μm; middle and right panels, 20 μm. (**B**) The presence of asbestos fibers inside adipocytes was detected using light microscopy at ×100 magnification (upper panel) and transmission electron microscopy (middle and lower panels). Scale bars: upper panel, 10 μm; middle panel, 5 μm; lower panel, 500 nm. (**C**) The cytotoxicity of asbestos fibers on adipocytes, MeT-5A mesothelial cells and RAW264.7 macrophages was measured by the adenosine triphosphate cell viability assay. All the cells were exposed to 10 μg/cm^2 of asbestos fibers for 72 h. The results are shown as the mean ± SEM of three independent experiments. *$P \leq 0.05$, **$P \leq 0.005$. Amo, amosite; Chry, chrysotile; Cro, crocidolite.

medium containing MTT was then aspirated from the wells, followed by the addition of 100 µl of dimethyl sulfoxide into each well to dissolve the purple formazan crystals. The optical density was measured using a PowerScan4 plate reader.

Wound-healing assay

MeT-5A, Y-MESO-8A or Y-MESO-8D cells were grown in a 6-well tissue culture plate until the cells formed a confluent monolayer. A scratch was then made across the cell monolayer using a pipette tip. Recombinant human MCP-1 was added to some of the wells at a concentration of 500 ng/ml. Images of the wound were taken immediately after the scratch (designated as 0 h) and at 18, 24 and 48 h after the scratch. The width of the wound was measured using ImageJ software, and the percentage of wound healing was then calculated.

Statistical analysis

The statistical significance between two groups of interest was analyzed using the unpaired Student's *t*-test. A P value of <0.05 was considered significant.

Table I. Top 20 genes upregulated in asbestos-treated cultured adipocytes

Gene name	Accession number	Fold change
Top 20 genes upregulated in chrysotile-treated adipocytes		
Prolactin family 2, subfamily c, member 5 (Prl2c5)	NM_181852	18.596165
Fibrinogen-like protein-1 (Fgl1)	BC029734	8.48526
Chemokine (C-C motif) ligand 2 (Ccl2)	NM_011333	8.051252
Troponin T2, cardiac (Tnnt2), transcript variant 9	NM_011619	6.9297132
Prolactin family 2, subfamily c, member 1 (Prl2c1)	NM_001045532	6.292936
Secreted phosphoprotein 1 (Spp1)	NM_009263	5.334665
High-mobility group AT-hook 2 (Hmga2)	NM_010441	5.1633744
Chemokine (C-C motif) ligand 8 (Ccl8)	NM_021443	4.867768
lincRNA:chr19:9060613-9060851 forward strand		4.497705
Fos-like antigen 1 (Fosl1)	NM_010235	4.422233
Interleukin 1 receptor-like 1 (Il1rl1), transcript variant 1	NM_001025602	4.192457
Tumor necrosis factor receptor superfamily, member 9 (Tnfrsf9), transcript variant 1	NM_011612	4.0868807
Plasminogen activator, urokinase (Plau)	NM_008873	4.038391
Runt-related transcription factor 1 (Runx1), transcript variant 2	NM_001111022	3.8444314
Interleukin 1 receptor-like 1 (Il1rl1), transcript variant 2	NM_010743	3.7691207
cDNA sequence BC023744 (BC023744)	NM_001033311	3.6094844
Matrix metallopeptidase 10 (Mmp10)	NM_019471	3.6034727
Matrix metallopeptidase 13 (Mmp13)	NM_008607	3.5614529
Serine/threonine/tyrosine kinase 1 (Styk1)	NM_172891	3.4867864
Acyl-CoA synthetase bubblegum family member 1 (Acsbg1)	NM_053178	3.3379452
Top 20 genes upregulated in crocidolite-treated adipocytes		
Serum amyloid A 3 (Saa3)	NM_011315	21.692352
Haptoglobin (Hp)	NM_017370	11.54753
Dermokine (Dmkn), transcript variant 3	NM_001166173	9.095255
Suprabasin (Sbsn), transcript variant 1	NM_172205	7.677543
Secretory leukocyte peptidase inhibitor (Slpi)	NM_011414	6.6974707
Serine (or cysteine) peptidase inhibitor, clade A, member 3G (Serpina3g)	NM_009251	6.258521
PREDICTED: *Mus musculus* predicted gene, EG628900 (EG628900)	XM_893705	6.231637
Chemokine (C-C motif) ligand 2 (Ccl2)	NM_011333	5.961754
Chemokine (C-C motif) ligand 9 (Ccl9)	NM_011338	5.94364
Chitinase 3-like 1 (Chi3l1)	NM_007695	5.8167386
Lipocalin-2 (Lcn2)	NM_008491	5.732993
Chemokine (C-X-C motif) receptor 7 (Cxcr7)	NM_007722	5.6649795
Prolactin family 2, subfamily c, member 5 (Prl2c5)	NM_181852	5.511816
Complement component 4B (Childo blood group) (C4b)	NM_009780	5.504423
Serine (or cysteine) peptidase inhibitor, clade A, member 3H (Serpina3h)	NM_001034870	5.3198853
Runt-related transcription factor 1 (Runx1), transcript variant 4	NM_009821	5.090166
Triggering receptor expressed on myeloid cells 2 (Trem2)	NM_031254	4.8963866
Fibrinogen-like protein 1 (Fgl1)	NM_145594	4.8214192
Cannabinoid receptor 1 (brain) (Cnr1)	NM_007726	4.818088
Placental protein 11 related (Ppl1r), transcript variant 2	NM_001168693	4.759451
Top 12 genes upregulated in amosite-treated adipocytes		
Extended synaptotagmin-like protein 3 (Esyt3)	NM_177775	2.988655
Budding uninhibited by benzimidazoles 1 homolog (*Saccharomyces cerevisiae*) (Bub1)	NM_009772	2.4976056
Potassium inwardly rectifying channel, subfamily J, member 6 (Kcnj6)	NM_001025585	2.4706264
lincRNA:chr4:21683562-21694344 reverse strand		2.4663801
PREDICTED: *M.musculus* predicted gene, EG666955 (EG666955)	XM_001000153	2.3627758
lincRNA:chr2:75493715-75494227 reverse strand		2.3625197
Adult male tongue cDNA, RIKEN full-length enriched library, clone:2310006M14 product:hypothetical protein, full insert sequence	AK009188	2.271196
ATPase, Ca^{++} transporting, type 2C, member 2 (Atp2c2)	NM_026922	2.2707396
lincRNA:chr6:31017987-31174287 reverse strand		2.2265513
Adult male olfactory brain cDNA, RIKEN full-length enriched library, clone:6430601O08 product:similar to Pol protein (fragment) (*M.musculus*), full insert sequence	AK032580	2.2096734
lincRNA:chr19:59498190-59531390 reverse strand		2.1915858
lincRNA:chr17:27479404-27481770 forward strand		2.082444

ATPase, adenosine triphosphatase; cDNA, complementary DNA. Twelve genes with >2-fold change were selected for amosite.

Results

Uptake of asbestos fibers by cultured adipocytes

The 3T3-L1 preadipocyte cell line was used to generate mature adipocytes according to the standard differentiation protocol. Adipocytes were used for subsequent experiments 10–14 days after the initiation of differentiation. During differentiation, the adipocytes accumulated lipid droplets in the cytoplasm that stained red upon Oil Red O staining (Figure 1A). Three different types of asbestos fibers, chrysotile, crocidolite and amosite fibers, were added to the adipocytes, followed by the assessment of fiber uptake using a cell block and light microscopy. Fiber uptake by the adipocytes was observed for all the asbestos types (Figure 1B, upper panel). Our findings were further supported by transmission electron microscopy, which clearly demonstrated fiber internalization by adipocytes (Figure 1B, lower panel). High magnification revealed the structure of a vesicular membrane around the asbestos fibers.

Asbestos fibers induce cell death when administered to mesothelial cells and macrophages (7,29). We compared the cytotoxicity of asbestos fibers on the cultured adipocytes, MeT-5A mesothelial cells and RAW264.7 macrophages by exposing them to the same concentration of asbestos fibers (10 μg/cm^2). When we performed an adenosine triphosphate detection cell viability assay on these different cell types, we did not observe any cytotoxic effect of asbestos fibers on the adipocytes, which was in contrast to mesothelial cells and macrophages (Figure 1C).

Cultured adipocytes showed changes in gene expression after asbestos exposure

As noted above, we hypothesized that the endocrine function of adipose tissue is potentially affected by asbestos exposure. To screen for genes with altered expression in asbestos-exposed adipocytes, we performed microarray gene expression analysis on the total RNA isolated from adipocytes after 72 h of exposure to asbestos fibers (GEO accession no.: GSE42330). The microarray results are shown in Table I. The top 20 genes that were upregulated in adipocytes after exposure to the different types of asbestos fibers are listed. More information can be found in the Supplementary Tables 1–3, available at *Carcinogenesis* Online. Gene expression analysis revealed the upregulation of some inflammation-related genes in adipocytes following exposure to asbestos fibers, including serum amyloid A3, haptoglobin and urokinase-type plasminogen activator. More importantly, we found the upregulation of an important adipocytokine that is commonly reported to be upregulated in obesity and is responsible for the related chronic inflammation and associated metabolic complications: chemokine C-C motif ligand 2 (Ccl2), which is also known as MCP-1. Other members of the C-C motif chemokine family were also upregulated, such as Ccl6, Ccl8 and Ccl9. Another gene that was upregulated in both chrysotile- and crocidolite-treated adipocytes was Prl2c5, which belongs to the prolactin superfamily.

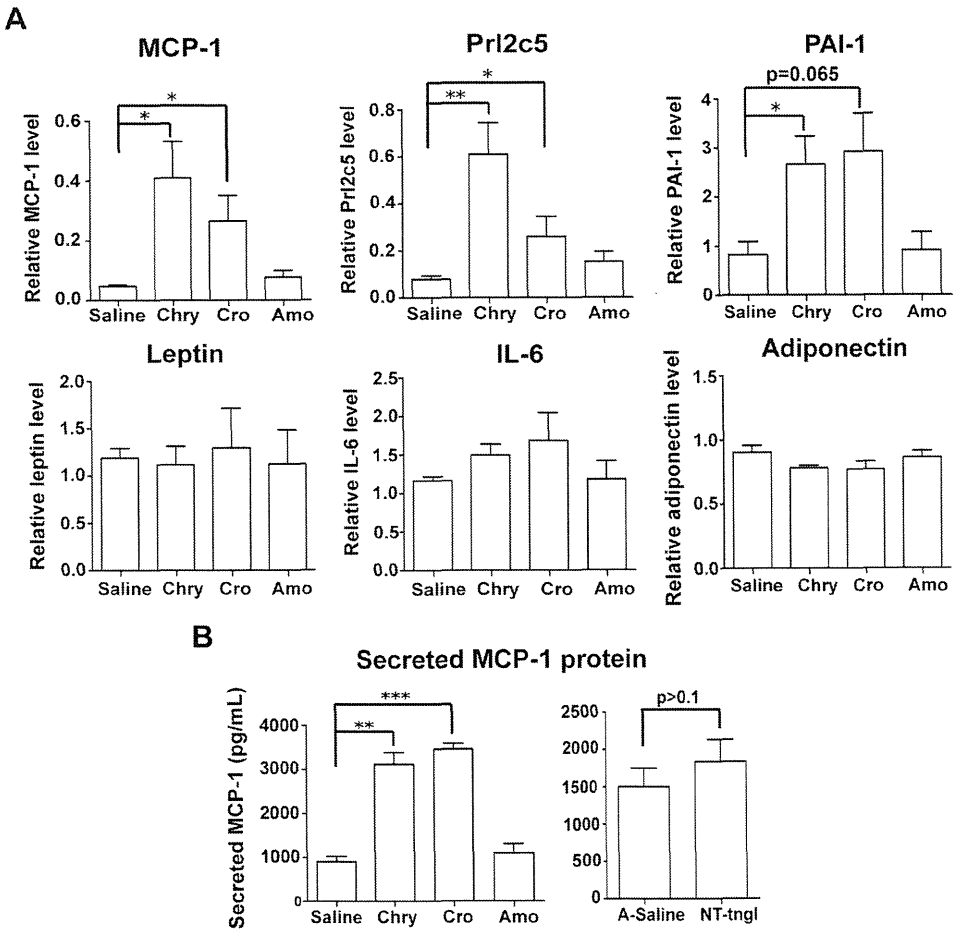

Fig. 2. Alterations in the expression level of adipocytokines in cultured adipocytes after asbestos exposure. Cultured adipocytes were exposed to chrysotile, crocidolite or amosite fibers at 10 μg/cm^2 for 72 h, with physiological saline as the control. (**A**) The gene expression level of various adipocytokines was measured by quantitative real-time RT–PCR and is shown relative to that of β-actin. (**B**) The secretion of MCP-1 into culture medium was measured by an MCP-1 immunoassay. In addition to asbestos fibers, adipocytes were also exposed to NT-tngl under the same experimental condition. The results are shown as the mean ± SEM of three independent experiments, $*P \leq 0.05$, $**P \leq 0.005$, $***P \leq 0.001$. Amo, amosite; A-Saline, saline containing 0.5% bovine serum albumin; Chry, chrysotile; Cro, crocidolite.

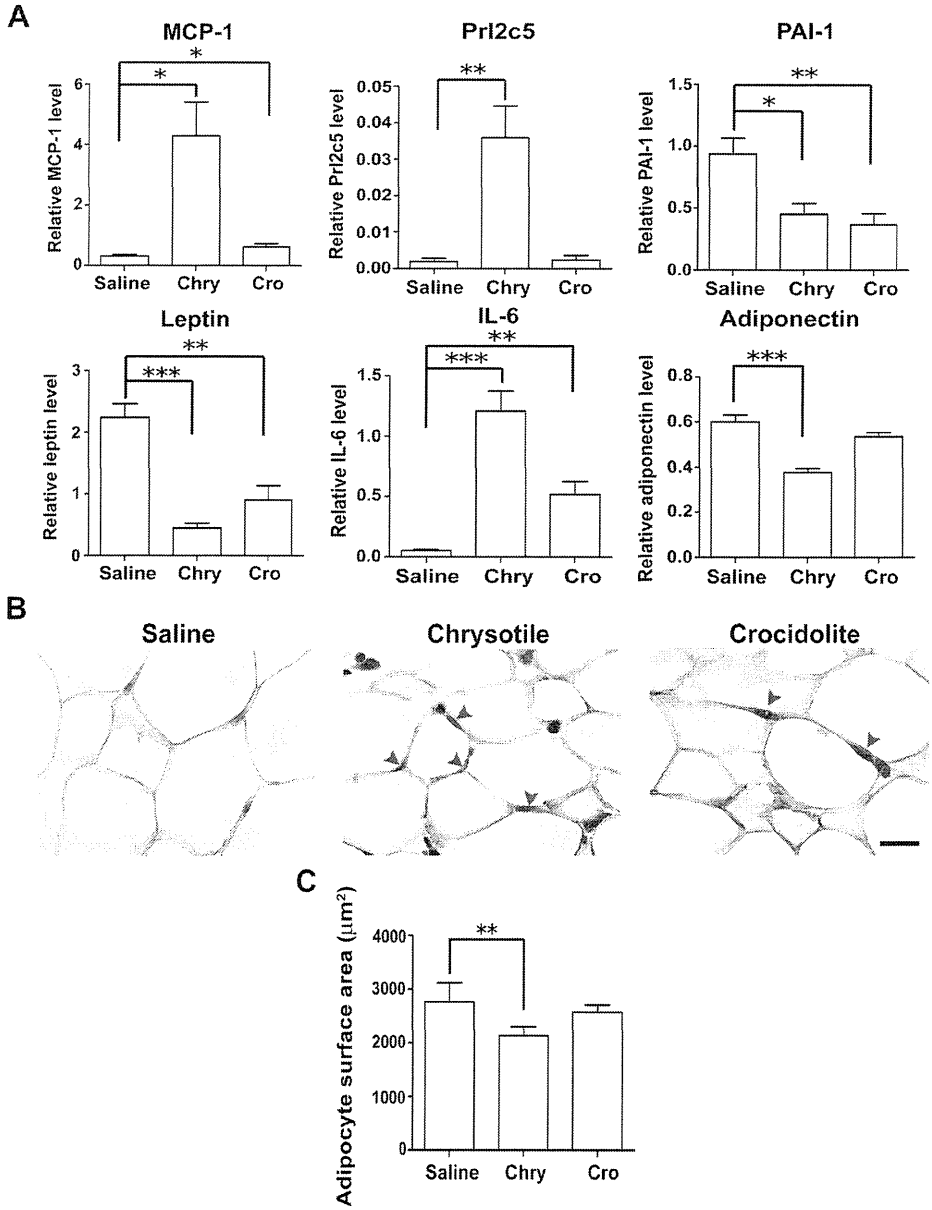

Fig. 3. Adipose tissues of mice injected with asbestos fibers show changes in adipocytokine expression levels. A total of 2.5 mg of chrysotile or crocidolite fibers was injected into the peritoneal cavity of mice, with physiological saline used as a control. Epididymal adipose tissue was harvested after 3 days. (**A**) The gene expression level of various adipocytokines in the epididymal adipose tissue was measured by quantitative real-time RT–PCR. The results are shown as the mean ± SEM (n = 6 per group). (**B**) Representative images of epididymal adipose tissue immunostained for MCP-1 expression. Scale bar: 20 μm. (**C**) Measurement of adipocyte cell surface area from adipose tissue sections using image analyzing software (n = 5 per group). $^{*}P \leq 0.05$, $^{**}P \leq 0.005$, $^{***}P \leq 0.001$. Chry, chrysotile; Cro, crocidolite.

MCP-1 was increased at the mRNA and protein level in adipocytes treated with asbestos fibers

Quantitative real-time reverse transcription–PCR (RT–PCR) was performed to evaluate the expression level of MCP-1, Prl2c5 and several other commonly known adipocytokines (PAI-1, leptin, IL-6 and adiponectin) in asbestos-treated or untreated adipocytes. In support of the microarray results, quantitative real-time RT–PCR showed the increased mRNA expression of MCP-1 and Prl2c5 in adipocytes following asbestos exposure (Figure 2A). Regarding the other adipocytokines examined, PAI-1 was also upregulated, whereas leptin, IL-6 and adiponectin did not show any significant alterations. Nevertheless, a slight decrease in adiponectin mRNA expression was observed. An enzyme-linked immunosorbent assay was performed to measure the secretion of MCP-1 protein into the culture medium of adipocytes treated with asbestos fibers. The enzyme-linked immunosorbent assay results corroborated those of quantitative real-time RT–PCR, showing a significant elevation of MCP-1 secretion by adipocytes treated with chrysotile and crocidolite fibers (control = 900.7 pg/ml, chrysotile treated = 3116.5 pg/ml, crocidolite treated = 3455.9 pg/ml, $P \leq 0.005$) (Figure 2B, left panel). Amosite-treated adipocytes did not show any apparent change in MCP-1 expression at either the mRNA or protein level. To determine whether any type of particulate is able to induce the same response, we also exposed the adipocytes to NT-tngl. Exposure to NT-tngl did not induce any significant increase in MCP-1 secretion from the adipocytes (Figure 2B, right panel).

Asbestos fibers dysregulated adipocytokine levels in adipose tissue of asbestos-exposed mice

To determine whether adipose tissue in living animals also responds to asbestos exposure, we injected chrysotile or crocidolite fibers into the peritoneal cavity of mice, with physiological saline as a control. Epididymal fat pads were harvested after 3 days, followed by quantitative real-time RT–PCR to examine changes in the expression level of adipocytokines. Again, the mRNA levels of MCP-1 and Prl2c5 were both upregulated in the adipose tissue of mice injected with asbestos fibers (Figure 3A). Regarding adiponectin, its suppressed expression level in the adipose tissue was more apparent than in the cultured adipocytes and was significant in chrysotile-injected mice. Leptin and IL-6 were significantly downregulated and upregulated, respectively, although no significant change in these two genes was observed in cultured adipocytes (Figure 2A). PAI-1 was the only exception that showed contradictory results between *in vitro* and *in vivo* assays. Immunohistochemical staining for MCP-1 and IL-6 was also performed on the adipose tissue sections. We found that in both chrysotile and crocidolite-injected mice, there was more intense MCP-1 staining in the cytoplasm of adipocytes compared with the saline-injected mice (Figure 3B). In contrast, the adipocytes did not show apparent positive staining of IL-6 (Supplementary Figure 1, available at *Carcinogenesis* Online), indicating that other inflammatory cells might be responsible for IL-6 mRNA upregulation as shown in Figure 3A. We have also noted some changes in adipocyte size and measurement of adipocyte surface area revealed a reduction of adipocyte size in asbestos-injected mice (Figure 3C).

MCP-1 promoted cancer cell phenotypes of mesothelial cells

Based on the well-known effect of MCP-1 as a macrophage chemoattractant, the increased secretion of MCP-1 by adipocytes in response to asbestos fibers might implicate an important indirect role of adipose tissue in enhancing the recruitment of macrophages to the sites of asbestos deposition. We collected culture media from asbestos-treated adipocytes and examined the ability of these conditioned media to induce macrophage migration. The transwell migration assay results revealed an increase in macrophage migration in response to the conditioned media from asbestos-treated adipocytes, which was most probably mediated by increased MCP-1 secretion (Figure 4).

Many chemokines have been reported to exert a mitogenic effect and are thus able to promote cancer development. We studied the effect of MCP-1 on mesothelial cell proliferation by treating MeT-5A cells with recombinant MCP-1 protein. MCP-1 showed a marginal but not significant effect on mesothelial cell proliferation (Figure 5A). In addition, we assayed the effect of MCP-1 on mesothelial cell migration. A wound-healing assay was performed in MeT-5A cells in the presence or absence of recombinant MCP-1 protein. We did not observe any effect of MCP-1 on MeT-5A cell migration (Figure 5B, left panel). However, we found that MCP-1 promoted the migration of the human mesothelioma cells Y-MESO-8A and Y-MESO-8D (Figure 5B, middle and right panels).

Discussion

Our results revealed for the first time that asbestos fibers are able to directly affect the endocrine activity of adipocytes. This effect might be mediated through a direct interaction, as we showed that adipocytes were able to phagocytose asbestos fibers. Although adipose tissue is more abundant in the peritoneal cavity, it is also present in the pleural cavity, e.g. submesothelial space of the parietal pleura, around the pericardial sac and near the mediastinum (30,31). These anatomic locations render relevance of adipose tissue as it is accessible for the inhaled fibers through fiber translocation. In response to asbestos exposure, adipocytes upregulated proinflammatory adipocytokine such as MCP-1 but suppressed the level of anti-inflammatory

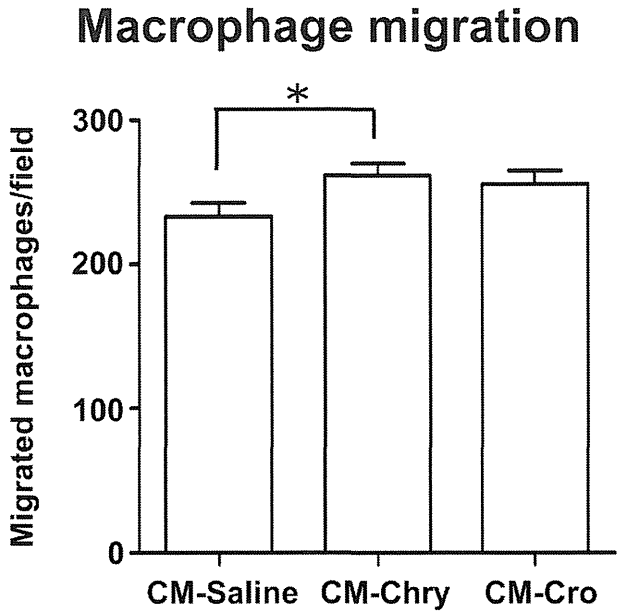

Fig. 4. Adipocytes induce increased macrophage migration following asbestos exposure. Cultured adipocytes were exposed to chrysotile or crocidolite fibers at 10 μg/cm^2 for 72 h, with physiological saline as a control. Conditioned medium was collected and assayed with a transwell migration assay to determine the ability of the conditioned media to induce macrophage migration. The results are shown as the mean ± SEM of three independent experiments. *$P \leq 0.05$. Chry, chrysotile; CM, conditioned medium; Cro, crocidolite.

adipocytokine, adiponectin, thereby shifting the balance towards a proinflammatory condition. Increased MCP-1 secretion by adipocytes might result in enhanced macrophage recruitment which in turn elaborates various cytokines and chemokines, leading to a vicious cycle that aggravates inflammation. Our results using adipocyte conditioned media to induce macrophage migration supported this notion. The role of adipose tissue in asbestos-induced inflammation can thus be both direct and indirect. MCP-1 has been reported to induce the proliferation of primary human pleural mesothelial cells (32) and our results using MeT-5A are consistent with the report. We also showed that MCP-1 promoted the migration of human mesothelioma cells. In addition, we observed a reduction in adipocyte size in asbestos-injected mice, which is probably due to the more active state of the adipocytes that requires higher metabolic rate.

MCP-1 transgenic and MCP-1$^{-/-}$ mice have previously been generated and characterized. MCP-1 overexpression in specific organs resulted in the enhanced recruitment of blood monocytes into the parenchyma of these organs (33,34). In contrast, in MCP$^{-/-}$ mice, there is a reduction in mononuclear cell infiltrate when these mice are challenged with different inflammatory stimuli (35). These mouse models are often used in studies related to obesity and insulin resistance. Kanda *et al.* (24) generated adipose-specific MCP-1 transgenic mice characterized by insulin resistance, hepatic steatosis and a higher degree of macrophage infiltration into adipose tissue. These MCP-1 genetically engineered mice might be a useful tool in our further studies to establish an association between MCP-1 expression and asbestos-induced mesotheliomagenesis.

In this study, we primarily focused on the possible tumor-promoting effects of MCP-1. Other adipocytokines with dysregulated expression might also play a cancer-promoting role. For instance, adiponectin expression is inversely correlated with human cancers. Low circulating levels of adiponectin have been associated with an increased risk of several cancers, such as colorectal cancer (36), endometrial cancer (37), postmenopausal breast cancer (38), gastric cancer (39) and prostate cancer (40). Adiponectin was reported to be able to inhibit the transcription factor nuclear factor-κB (41,42), which is